JOURNAL OF GEOPHYSICAL RESEARCH, VOL. 115, C07011, doi:10.1029/2009JC005837, 2010

Optical complexity in Long Island Sound and implications for coastal ocean color remote sensing

D. A. Aurin,[1] H. M. Dierssen,[1] M. S. Twardowski,[2] and C. S. Roesler[3]

Received 23 September 2009; revised 18 December 2009; accepted 8 January 2010; published 17 July 2010.

[1] The optical properties of estuaries can vary considerably with the delivery of pigmented materials from surrounding watersheds and marine waters. In this study, optical properties sampled at 158 stations throughout the Long Island Sound (LIS) estuary between 2004 and 2007 show significant regional variability. Chlorophyll, total suspended matter, light absorption, and scattering are exceptionally high compared to other coastal data. Inherent optical properties and sea surface reflectances revealed at least two optical domains: a phytoplankton-dominated regime in western LIS and New York Bight and a sediment-dominated regime in central and eastern LIS. Multivariate ordination analysis identified clusters of stations conforming to these optical domains, as well as stations near the Hudson and Connecticut rivers representing optical end-members in LIS characterized by high chromophoric dissolved material (CDM) and biomass (Hudson River) and high sediment loads (Connecticut River). However, winds, tides, and subtidal estuarine circulation redistribute optical constituents throughout the major basins of LIS and homogenize riverine influence. Ocean color parameters, used to define the spectral quality of optical constituents, such as the spectral slopes of particulate backscattering and CDM absorption, and the chlorophyll-specific phytoplankton absorption did not cluster and are relatively constant throughout the region at all times of year. Therefore, variability in spectral reflectance in LIS is principally controlled by the relative magnitudes of the optical properties at each station rather than by significant differences in spectral quality of optically significant constituents. Consistency in these ocean color parameters minimizes the necessity for subregional or seasonal "tuning" of ocean color algorithms.

Citation: Aurin, D. A., H. M. Dierssen, M. S. Twardowski, and C. S. Roesler (2010), Optical complexity in Long Island Sound and implications for coastal ocean color remote sensing, *J. Geophys. Res.*, *115*, C07011, doi:10.1029/2009JC005837.

1. Introduction

[2] Variability in optical properties and biogeochemical constituents tends to be high in the coastal zone as a result of localized dynamics and variability in the sources of particulate and dissolved materials [*Bricaud et al.*, 1995; *Coleman*, 1999; *Astoreca et al.*, 2006; *Brando et al.*, 2006]. For instance, *Oubelkheir et al.* [2006] recently reported 2 orders of magnitude variability in the particle scattering and dissolved absorption in the macrotidal waters extending from the Fitzroy Estuary to the Keppel Bay in northeastern Australia, while the backscattering efficiency varied as much as a factor of 6 across the same region. *Chang et al.* [2007] ascribed large variability in optical properties and chlorophyll concentration in the Santa Barbara Channel to localized seasonal events such as river plumes, storm events and upwelling. Such optical variability presents distinct challenges to ocean color remote sensing algorithm parameterization and performance, particularly in an optically complex estuary such as Long Island Sound. Overcoming these challenges requires that optical variability is understood in the context of driving physical and biological dynamics of a region.

[3] The inherent optical properties (IOPs) of the water column depend on the composition, concentration and size of suspended particles and dissolved material in the water column (see Table 1 for abbreviations). Inversely, water column optical properties are proxies to important biogeochemical properties such as phytoplankton biomass, pigment concentration (e.g., chlorophyll a concentration, Chl), total suspended material (TSM), and particle size distribution (PSD), while they can also determine light availability at depth and solar heat flux [*Morel and Bricaud*, 1981; *Kitchen et al.*, 1982; *Gordon and Morel*, 1983; *Kirk*, 1994; *Mobley*, 1994]. The magnitudes of the absorption $a(\lambda)$, scattering $b(\lambda)$, and attenuation $c(\lambda)$ coefficients (where λ is wavelength) are proportional to the concentrations of various dissolved and suspended particulate constituents in the water column. In fact, the IOPs can be related to biogeochemical properties provided the specific IOPs (i.e., optical

[1]Department of Marine Sciences, University of Connecticut, Groton, Connecticut, USA.
[2]WET Labs Inc., Narragansett, Rhode Island, USA.
[3]Department of Geology, Bowdoin College, Brunswick, Maine, USA.

0148-0227/10/2009JC005837

Table 1. Summary of Abbreviations and Acronyms

	Units	Definition
$a(\lambda)$	m^{-1}	Total absorption coefficient
$a_{cdm}(\lambda)$	m^{-1}	CDM (or gelbstoff) absorption coefficient
$a_{\min}(\lambda)$	m^{-1}	Mineral absorption coefficient
$a_{nap}(\lambda)$	m^{-1}	NAP absorption coefficient
$a_p(\lambda)$	m^{-1}	Particulate absorption coefficient
$a_\varphi(\lambda)$	m^{-1}	Phytoplankton absorption coefficient
$a_\varphi^*(\lambda)$	m^2 (mg Chl a)$^{-1}$	Specific phytoplankton absorption coefficient
$a_w(\lambda,T,S)$	m^{-1}	Pure seawater absorption coefficient
$b(\lambda)$, $b_p(\lambda)$	m^{-1}	Total, particulate scattering coefficient
$b_{bp}(\lambda)$	m^{-1}	Particulate backscattering coefficient
$\tilde{b}_{bp}$ (λ)		Particulate backscattering ratio (b_{bp}/b_p)
$c(\lambda)$, $c_p(\lambda)$	m^{-1}	Total, particulate attenuation coefficient
$E_s(\lambda)$	W m^{-2} nm^{-1}	Downwelling surface irradiance
$L_u(\lambda,z)$, $L_w(\lambda)$	W m^{-2} nm^{-1} sr^{-1}	Upwelling, water-leaving radiance
n_p		Bulk particulate refractive index (relative to seawater)
$R_{rs}(\lambda)$	sr^{-1}	Remote sensing reflectance
S	Psu	Salinity
S_{cdm}, S_{cdm}'	nm^{-1}	Exponential slope of a_{cdm}, Power law slope of a_{cdm}
S_{nap}	nm^{-1}	Exponential slope of a_{nap}
T	°C	Temperature
Y		Power law slope of b_{bp}
z	M	Depth
β (λ, θ)	m^{-1}	Volume scattering function
γ		Power law slope of c_p
ξ		Power law slope of PSD
λ, λ_0	Nm	Wavelength, reference wavelength
χ		Constant relating β to b_b
CDM		Colored Dissolved Material
Chl	mg m^{-3}	Chlorophyll a concentration
CTR		Connecticut River
(E-,C-,W-) LIS		(Eastern, central, western) Long Island Sound
NAP		Nonalgal material
NOMAD		NASA Bio-optical Marine Algorithm Data Set
NYB		New York Bight
PSD	particles ml^{-1} μm^{-1}	Particle size distribution
SAA		Semianalytical ocean color algorithm
TSM	g m^{-3}	Total suspended material

property per unit constituent concentration) are known. Each IOP can be linearly separated into dissolved, nonalgal particulate (NAP), and phytoplankton components. In coastal and estuarine waters, variability in nutrient abundance and sunlight, riverine and tidal sources of chromophoric dissolved material (CDM) and suspended sediments, and episodic wind-wave-driven particle resuspension drive high variability in IOPs such as phytoplankton absorption, $a_\varphi(\lambda)$, CDM absorption, $a_{cdm}(\lambda)$, NAP absorption, $a_{nap}(\lambda)$ and scattering (e.g., particle scattering, $b_p(\lambda)$, and scattering in the backward direction, $b_{bp}(\lambda)$). Similarly, variability in the specific IOPs, e.g., $a_\varphi^*(\lambda) = a_\varphi(\lambda)$/Chl, may be high owing to changes in phytoplankton speciation and/or physiological state (i.e., changes in pigmentation), or changes in pigment packaging. Variability in other specific IOPs, such as the dissolved organic material-specific CDM absorption and the particulate organic carbon-specific particle attenuation have also been well documented [*Oubelkheir et al.*, 2006, and references therein].

[4] Ocean color remote sensing algorithms operate on the principle that as sunlight passes into and is reflected back from the water column, changes in its spectral quality (i.e., its color) and intensity depend upon the optical constituents in the water. Specifically, the spectral shape and magnitude of the remote sensing reflectance $R_{rs}(\lambda)$ are related to the IOPs in the water column [*Morel and Prieur*, 1977]. Given certain empirical approximations, semianalytical ocean color algorithms (SAAs) invert $R_{rs}(\lambda)$ for retrieval of IOPs and biogeochemical properties [*Zaneveld et al.*, 2006]. Several SAAs have been developed for waters with high particle loads and turbidity, as well as strong CDM absorption, and various types and sizes of phytoplankton and minerogenic material, i.e., optically complex, or "Case 2" waters in which optical properties are significantly influenced by minerals and CDM, whose concentrations do not covary with the phytoplankton [e.g., *Gordon and Morel*, 1983; *Roesler and Perry*, 1995; *Garver and Siegel*, 1997; *Carder et al.*, 1999; *Lee et al.*, 2002; *Maritorena et al.*, 2002; *Van Der Woerd and Pasterkamp*, 2008]. In order for these algorithms to accurately retrieve IOPs and biogeochemical properties in complex waters, they may require regional parameterization to accommodate large variability in optical properties, specific optical properties, and other ocean color parameters.

[5] Ocean color parameters describing the spectral shape of IOPs, the slope of the PSD, the particle backscattering ratio ($\tilde{b}_{bp} = b_{bp}/b_p$), and relationships between inherent optical properties and biogeochemical quantities (e.g., $a_\varphi^*(\lambda)$), are related to the composition and morphology of particulate and dissolved materials in the water column. For example, *Twardowski and Donaghay* [2001] described a method for estimating the bulk particulate refractive index (relative to

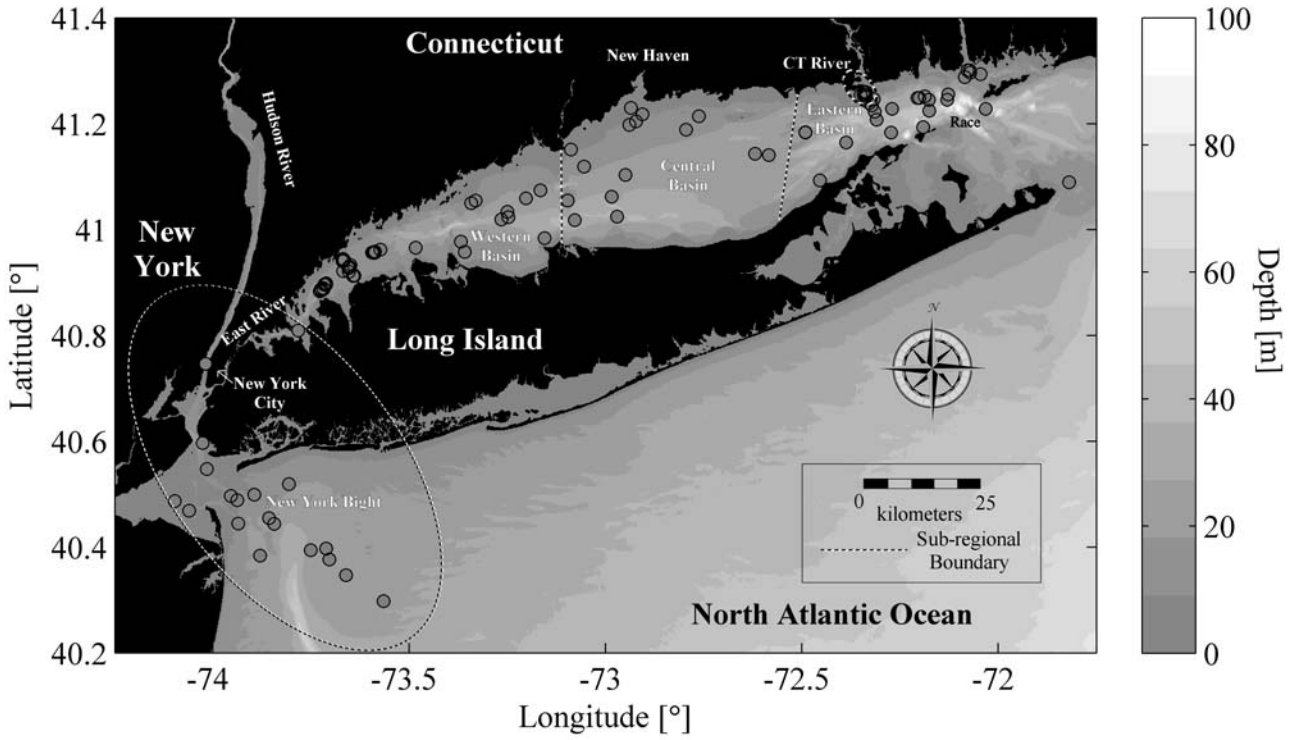

Figure 1. Map of the study area showing stations sampled between 2004 and 2007 (dots) and subregional boundaries (dotted line, names in gray). Bathymetry is contoured in gray scale.

water) using the slope of PSD, ξ (or the spectral slope of c_p, γ), together with $\tilde{b}_{bp}$. The spectral slope of CDM, S_{cdm}, can be related to the chemical composition (i.e., humic acid to fulvic acid ratio [*Carder et al.*, 1989]) and its relation to the origin of the organic material [e.g., *Bricaud et al.*, 1981; *Roesler et al.*, 1989] and photooxidation state [*Mopper et al.*, 1991]. Pigment composition, community structure, and physiological condition of phytoplankton can be estimated from a_φ* [*Morel and Bricaud*, 1981; *Roesler et al.*, 1989; *Ciotti et al.*, 2002; *Moore et al.*, 2005]. Regional parameterization of SAAs often depends on characterization of these and other ocean color parameters to achieve accurate retrievals of IOPs and biogeochemical properties.

[6] Here, we evaluate the optical properties of Long Island Sound (LIS, Figure 1) which stretches about 177 km to the east of New York City, is 34 km wide at its widest point, and averages 24 m in depth. Water flows into LIS from the nutrient rich Hudson River (i.e., by way of the East River) at the head of the estuary, from the sediment laden Connecticut River (the largest of many rivers draining into LIS), and from the comparatively clear shelf waters east of the Race (Figure 1). Each of these end-members has distinctive optical qualities, but strong tidal and subtidal exchange mix these waters in ways which are only now beginning to become clear through increased observatory and ferry sampling efforts [*Codiga and Aurin*, 2007; *O'Donnell et al.*, 2007]. The distribution of optical and biogeochemical properties is further complicated by nonfluvial coastal influences, such as episodic wave driven resuspension of sediments and wastewater discharge, at this gently sloping, sediment-rich continental margin.

[7] Unlike most estuaries, LIS receives most (>70%) of its riverine input from the Connecticut River just 20 km from the mouth of the estuary [*Blumberg and Pritchard*, 1997; *Gay et al.*, 2004]. Exchange between the estuary and shelf waters at the mouth of LIS (i.e., the Race, Figure 1) is driven by semidiurnal flushing and vigorous subtidal exchange [*Codiga and Aurin*, 2007]. Studies of other estuaries, such as *Blondeau-Patissier et al.* [2009] in northeastern Australia, have suggested that multiple distinct optical domains (i.e., water masses having similar spectral characteristics in their optical properties and specific IOPs) may occur within a river-estuary-ocean mixing region, and that regionally averaged values of ocean color parameters may not adequately represent these water types. This study aims to address whether such optical domains may be found within LIS, or whether robust mixing may lead to widespread homogenization of optical properties and/or ocean color parameters between the riverine and shelf water end-members.

[8] The earliest treatment of the optical properties of LIS in the literature dates back to *Morrison*'s [1970] study, and several studies have included optical data from LIS since then [*Leathers et al.*, 1999; *Gardner et al.*, 2001; *Sosik et al.*, 2001; *Morrison and Sosik*, 2002; *Werdell and Roesler*, 2003; *Etheridge and Roesler*, 2004; *Branco and Kremer*, 2005; *Ackleson*, 2006]. Time series profiles of IOPs at the Race in 2000 and 2001 [*Morrison and Sosik*, 2002] showed twofold variability in the absorption properties of surface

waters associated with tidal transport. Previous studies have focused on highly localized areas within LIS, and do not address broader spatial or temporal trends in multiple IOPs, radiometric properties, or ocean color parameters. Here, we characterize optical properties and ocean color parameters throughout the major basins of LIS, and their influence on the sea surface spectral reflectance. We explore sources of turbidity (e.g., phytoplankton and suspended sediment distribution) and CDM compared with other coastal and estuarine data sets, and address the variability in the quantity and quality of optical constituents throughout the region both spatially and seasonally.

2. Data and Methodology

2.1. Field Data Overview

[9] Broadly speaking, LIS can be broken into three major basins (eastern, central and western; ELIS, CLIS, and WLIS, respectively, Figure 1) based on watershed [*Burg*, 2008] and circulation [*Riley*, 1956]. Two additional subregions accommodate stations sampled within and adjacent to the two largest fresh water sources in the region: the Hudson and Connecticut rivers. The first, collectively referred to here as New York Bight (NYB), comprises any stations sampled in the Hudson River, New York Harbor, the East River, Raritan Bay or New York Bight. While these stations are not technically within LIS, they are included here because of the strong influence these waters have on the western Narrows and WLIS in general. The second encompasses all stations sampled within 1.5 km of the mouth of the Connecticut River (CTR). Within these two subregions (CTR and NYB), plume stations (CTRp and NYBp) are identified based on a combination of factors, including vertical salinity gradient strength, $\tilde{b}_{bp}$, change in ξ with depth, "brownness" of the surface waters as measured by R_{rs}, and visual confirmation of the plume structure from field notes. It should be noted that NYBp stations include stations sampled in the NYB and WLIS geographic regions, since both are associated with Hudson River plume waters.

[10] Field measurements for this study comprise $R_{rs}(\lambda)$, IOPs, Chl, PSD, TSM and ancillary data collected at 158 stations during twelve cruises between May 2004 and December 2007 (Table 2). Each component of the field data has a unique protocol for processing, binning, weighting, merging, etc., sometimes requiring interdependent and/or iterative processing. We therefore have included two flowcharts (Figures 2a and 2b) to clarify and summarize the methodology description that follows. Comparisons are made with the NASA Bio-optical Marine Algorithm Data Set (NOMAD), an archive of marine optical measurements from over 3,400 predominantly coastal stations worldwide [*Werdell and Bailey*, 2005], as well as numerous other coastal studies in North America, Europe, and Australia.

2.2. Optical, Biogeochemical, and Ancillary Measurements

[11] The dissolved absorption coefficient, a_{cdm}, the total nonwater absorption coefficient ($a_{pg} = a - a_w$), and the total nonwater attenuation coefficient, c_{pg}, were measured with a profiling platform at a minimum of nine wavelengths, while the backscattering coefficient was generally measured only at 660 nm (exceptions are explained below). Spectral whole and 0.2 μm filtered absorption and attenuation were measured with the ac-9 or ac-S (WET Labs) instruments. The backscattering coefficient was most frequently measured with the BBFL2 or BB3 (WET Labs) instruments, although limited multispectral observations were made using the Hydroscat-6 (Hobilabs). Temperature, conductivity and pressure were measured using a CTD (SBE25 or SBE49, Seabird).

[12] Absorption and attenuation measurements were visually inspected to eliminate bubble contamination, and corrected for time lag associated with flow rate through the ac-9/ac-S. Absorption and attenuation measurements were further corrected for instrument drift, temperature, salinity [*Sullivan et al.*, 2006; *Twardowski et al.*, 1999] and a proportional scattering correction [*Zaneveld et al.*, 1994] was applied. The exponential slope of a_{cdm}

$$a_{cdm}(\lambda) = a_{cdm}(\lambda_0)\exp(S_{cdm}(\lambda_0 - \lambda)) \quad (1)$$

(where λ_0 is a reference wavelength) was calculated by fitting a_{cdm} data between 412 nm and 650 nm to equation (1) in a least square, nonlinear sense. Attenuation spectral slope γ was calculated using a powerlaw model for particulate attenuation

$$c_p(\lambda) = c_p(\lambda_0)\,(\lambda/\lambda_0)^{-\gamma} \quad . \quad (2)$$

Volume scattering, β, measurements from WET Labs backscattering instruments were corrected for total absorption along the path length, and particulate backscattering b_{bp} was calculated following *Boss et al.* [2001]. A χ factor of 0.9 was used [*Sullivan et al.*, 2005]; however, published values generally range from 0.9 – 1.1 [*Boss and Pegau*, 2001]. Uncertainty in the phase function estimated from single angle sensors can introduce large errors (~20%) into estimates of b_{bp}. Backscattering spectral slope Y was calculated by fitting b_p to a power law model in a least square, nonlinear sense between 412 nm and 650 nm, and assuming a spectrally flat $\tilde{b}_{bp}$ [*Ulloa et al.*, 1994; *Whitmire et al.*, 2007]. The backscattering spectral slope was used to extrapolate backscattering measurements at 660 nm to 650 nm and 555 nm for comparison with other instruments and data sets. Optical profile data were binned to 0.5 m. Weighted surface average values of IOPs were estimated following *Zaneveld et al.* [2005] using the radiative transfer software Hydrolight (Sequoia Scientific) to model the radiant light field.

[13] Particle size distribution was measured using a LISST-100X (Sequoia Scientific) and processed to particle volume concentration using the software provided by Sequoia Scientific. The particle concentration was calculated from the volumetric concentration assuming spherical particles in the assemblage (particles L^{-1}). Total particle concentrations were estimated as the sum of the particle concentration across the size range from 6.07 and 230.98 μm (C. J. Buonassissi and H. M. Dierssen, A regional comparison of particle size distributions and the power-law approximation in oceanic and estuarine surface waters, submitted to *Journal of Geophysical Research*, 2009). The particle size distribution, *dN/dD* (particles L^{-1} μm^{-1}, where D is particle diameter), was estimated by normalizing the particle concentration (N) by the width of each logarithmically spaced size bin. The

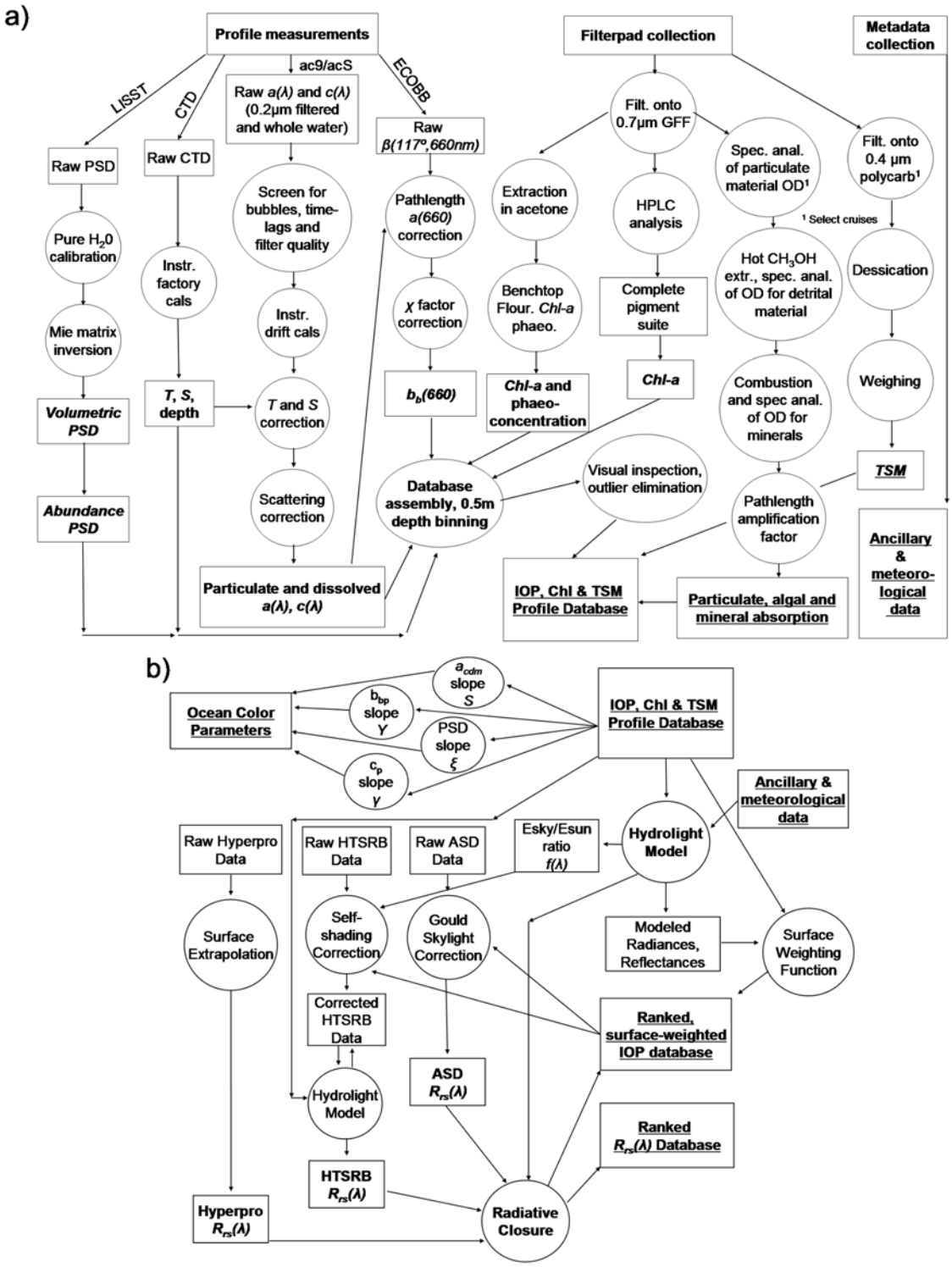

Figure 2. Data collection and data processing are shown as flowcharts to highlight the interdependency between multiple instruments and platforms in a comprehensive IOP/AOP data set such as this. Rectangles enclose data, circles enclose processing components. (a) Flowchart for profiled measurements, discrete measurements, ancillary data and metadata. (b) Flowchart for ocean color parameters, R_{rs}, surface weighting, and radiative closure.

Table 2. Field Cruises[a]

Cruise	Date	Stations	Subregions				
			1	2	3	4	5
OGCO04	4 May	23	X	X	X	X	
LISICOS0305	5 Mar	9			X		
OGCO05	5 May	32	X	X	X	X	X
LISICOS0705	5 Jul	33					
LIS0106	6 Jan	2	X				
LISICOS0306	6 Mar	5			X		
LISICOS0406	6 Apr	3			X		
OCGO06	6 Jul	31	X	X	X	X	X
LISICOS0806	6 Aug	11			X		
LIS0507	7 Jun	3	X			X	
LIS0707	7 Jul	3	X			X	
LIS1207	7 Dec	3	X			X	

[a]Subregions sampled during each cruise (1, eastern LIS; 2, central LIS; 3, western LIS; 4, Connecticut River; 5, New York Bight) are marked with an X.

PSD slope, ξ, was estimated from equation 3 using linear regression of the log-transformed variables

$$\frac{dN}{dD} \propto D^{-\xi}. \tag{3}$$

Discrete seawater samples were collected at each station at one or more depths and filtered onto Whatman GFF (nominal pore size 0.7 μm) filters. Filter pads were stored on dry ice while at sea, and then transferred to a −80°C freezer. Chl was determined fluorometrically [*Holm-Hansen et al.*, 1965]. At selected stations, the particulate, phytoplankton, nonalgal particulate, and minerogenic absorption coefficients ($a_p(\lambda)$, $a_\varphi(\lambda)$, $a_{nap}(\lambda)$, $a_{\min}(\lambda)$) were measured in a Cary 3E (Varian Inc.) or U-3010 (Hitachi Inc.) dual-beam spectrophotometer following NASA protocols [*Fargion and Mueller*, 2000] with a path length amplification factor of 2.0 [*Roesler*, 1998], and combustion to separate NAP into organic and mineral components [*Bowers et al.*, 1996; *Werdell and Roesler*, 2003]. TSM concentration was determined gravimetrically at selected stations during summertime cruises in 2005 and 2006 following the procedures outlined in NASA protocols [*Hooker et al.*, 1995].

2.3. Radiometric Measurements

[14] Hyperspectral (325 nm–1075 nm, 1 nm resolution) surface reflectance measurements were taken above the sea surface with a Fieldspec radiometer (Analytical Spectral Devices) and processed to remote sensing reflectance R_{rs} (defined here as water-leaving radiance L_w normalized to downwelling irradiance at the surface E_s; spectral notation suppressed) by removing sea surface glint and reflected skylight following *Gould et al.* [2001] parameterized for the coastal zone. Error in R_{rs} was estimated using variability between five replicate observations.

[15] During several cruises, R_{rs} was also estimated using Satlantic's Hyperpro (350 nm – 800 nm, ~3nm resolution) or HTSRB (350 nm – 800 nm, 1 nm resolution) instruments. Both of these instruments collect the upwelling radiances L_u below the sea surface and E_s from a sensor on the ship (Hyperpro) or a sensor atop the buoy (HTSRB). In the case of the HTSRB, L_u was measured at 0.65 m below the sea surface, while the Hyperpro profiled to below the euphotic zone (vertical resolution < ~ 0.25 m above 3 m; lower below that where low light levels lead to longer shutter integration times). Self-shading corrections were applied to data collected by the radiance sensor beneath the HTSRB buoy following *Leathers et al.* [1999] and *Gordon and Ding* [1992].

[16] In the case of the Hyperpro, L_u was extrapolated to immediately below the air-sea interface using a linear fit to a log-transformed profile (assuming a constant diffuse vertical attenuation coefficient in the surface layer), while error was estimated using the variability in E_s during the interval of extrapolation. Transmittance across the air-water interface was estimated following *Mobley* [1994]. Measured L_u at 0.65 m by the HTSRB was extrapolated to L_w using an iterative closure radiative modeling approach in which the total absorption and attenuation coefficients measured simultaneously at each station in profile (0.5 m bins) and ancillary data were used as inputs to the radiative transfer software Hydrolight. Hydrolight was run iteratively while adjusting the phase function, β, until the modeled upwelling radiance at 0.65 m matched that measured in situ (spectrally integrated difference < 10%). Error in R_{rs} measured by the HTSRB is estimated for each station using the standard deviation in L_u measured over the sampling period. Due to the highly turbid nature of LIS, the bottom depths of stations sampled, and the low albedo of bottom sediments generally found in LIS [*Werdell and Roesler*, 2003], all stations were considered optically deep with no bottom reflectance contributing to the surface signature.

2.4. Radiative Closure

[17] Inputs to the radiative transfer model, Hydrolight, included a_{pg} and c_{pg} at 0.5 m depth resolution and 9 wavelengths (412, 440, 488, 510, 532, 555, 650, 676, and 715 nm), median $\tilde{b}_{bp}$ at each station, and ancillary data (location, time, wind speed, and cloud cover). Pure water absorption values were estimated from *Pope and Fry* [1997], and a *Fournier and Forand* [1994] phase function was estimated in Hydrolight from the median backscattering ratio. Raman scattering was included in the model. Irradiance was estimated using the RADTRAN model [*Gregg and Carder*, 1990] together with ancillary data.

[18] Stations were evaluated for radiative closure by comparing measured R_{rs} and modeled $\hat{R}_{rs}$ using two novel metrics: a spectrally integrated R_{rs} magnitude percent difference, and a normalized, integrated R_{rs} shape percent difference. These were calculated as follows:

$$\Delta_{mag} = \frac{\int_{412}^{650} R_{rs}d\lambda - \int_{412}^{650} \hat{R}_{rs}d\lambda}{\int_{412}^{650} \hat{R}_{rs}d\lambda} * 100\%;$$

$$\Delta_{shape} = \frac{\int_{412}^{650} R_{rs}/R_{rs}(555)d\lambda - \int_{412}^{650} \hat{R}_{rs}/\hat{R}_{rs}(555)d\lambda}{\int_{412}^{650} \hat{R}_{rs}/\hat{R}_{rs}(555)d\lambda} * 100\%. \tag{4}$$

Finally, a weighted rank for closure was established between 0 (best quality) and 10 (worst quality), preferentially weighting differences in spectral shape over magnitude

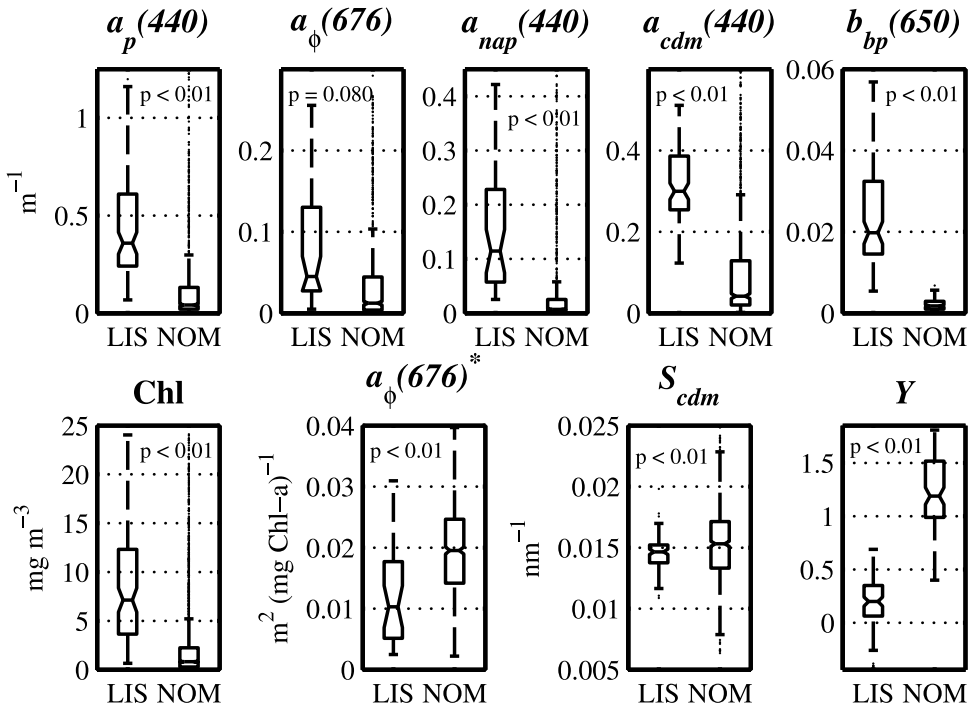

Figure 3. Inherent optical property magnitudes, chlorophyll a and ocean color parameters in the Long Island Sound (LIS) and NOMAD (NOM) data sets. Total particulate (a_p), nonalgal particulate (a_{nap}), and dissolved absorption (a_{cdm}) coefficients are shown at 440 nm. Phytoplankton absorption (a_φ) and specific absorption (a_φ*) are shown at 676 nm, and particulate backscattering (b_{bp}) at 650 nm. The p value for one-way ANOVA between data sets is displayed in each box-whisker plot. Outliers truncated for clarity.

differences, since these have a more significant impact on inversion algorithms

$$rank = \frac{2^*|\Delta_{shape}| + |\Delta_{mag}|}{30}, \quad (5)$$

where the denominator acts to scale our results between the ranks of 0 and 10.

2.5. Statistical Analysis

[19] One-way analysis of variance (ANOVA, critical p < 0.01 [*Hogg and Ledolter*, 1987]) in conjunction with Tukey-Kramer [*Kramer*, 1956] analysis (significance level 0.05) is used to compare IOPs, biogeochemical properties, and ocean color parameters between LIS and NOMAD data sets, and to evaluate differences in these properties seasonally and between subregions of LIS. Tukey-Kramer multiple comparison procedures provide an upper bound on the probability that any comparison between populations will be found significant, and is considered accurate even in the cases where populations may be correlated.

[20] To establish whether discrete optical domains exist in LIS, multivariate statistics are performed on collective measures of optical property magnitudes and spectral shape parameters using the computational software Matlab© (Mathworks). Prior to recasting data into ordinate space, observations are normalized by dividing the deviation of each data point from the mean of each data parameter by the standard deviation of that parameter (i.e., using the Matlab function zscore) in order to remove artifacts associated with differences in units which might otherwise distort data proximity calculations. A complete linkage hierarchical clustering is evaluated using Euclidean distances to identify stations with similar characteristics. Non-metric Multidimensional Scaling (NMDS), and Principal Component Analysis (PCA) are then applied to help visualize cluster linkages and distances between the many data variables sampled at each station given the clustering thresholds [*Gotelli and Ellison*, 2004]. These ordination techniques are designed to summarize multivariate data by plotting samples (i.e., field stations) with similar attributes close together when projected into two dimensional plots. Depending on a Euclidean distance threshold, samples are then assigned to discrete clusters of samples with similar attributes. Kruskal's stress test [*Kruskal and Wish*, 1978] is used to test the probability that NMDS arrived at a correct solution (i.e., stress < 0.1). In other words, it tests whether disparities resulting from the transformation of the data dissimilarities are large. Hierarchical clustering and multivariate statistics are evaluated first to identify similarities in data describing IOP magnitude, and second for data describing IOP spectral quality (i.e., ocean color parameters).

3. Results

3.1. Variability in Optical and Biogeochemical Properties

[21] The magnitudes of all major IOPs are significantly higher in LIS than those reported in NOMAD [*Werdell and Bailey*, 2005] (Table 3 and Figure 3). ANOVA analysis between the two data sets demonstrated that all parameters shown in Figure 3 are significantly different except a_φ (676).

Table 3. Summary of Surface Weighted IOPs and Optical Parameters

	Long Island Sound					
	Median	SD	Minimum	Maximum	n	NOMAD Median ± SD (n)
$a_p(440)$ (m^{-1})	0.36	0.32	0.07	1.63	110	0.04 ± 0.30 (864)
$a_{cdm}(440)$ (m^{-1})	0.30	0.10	0.12	0.75	110	0.04 ± 0.17 (814)
a_φ (440) (m^{-1})	0.072	0.126	0.008	0.478	43	0.03 ± 0.167 (833)
$a_{nap}(440)$ (m^{-1})	0.115	0.107	0.025	0.421	45	0.007 ± 0.15 (833)
$a_{min}(440)$ (m^{-1})	0.063	0.069	0.006	0.194	30	-
$b_p(440)$ (m^{-1})	2.00	1.41	0.39	11.28	110	-
$b_{bp}(660)$ (m^{-1})	0.019	0.020	0.006	0.124	97	0.002 ± 0.001 (184)
$c_p(440)$ (m^{-1})	2.47	1.64	0.47	12.56	110	-
Chl (mg m^{-3})	7.1	12.0	0.7	80.6	121	0.8 ± 5.7 (3032)
TSM (g m^{-3})	2.9	1.9	0.7	10.3	46[a]	-
PSD(37μm) (ml^{-1})	11.57	11.00	0.70	94.08	2809[a]	-
a_φ (676)[b] (m^2 mg^{-1})	0.010	0.009	0.002	0.042	33	0.02 ± 0.01 (833)[b]
$b_{bp}/b_p(555)$	0.013	0.008	0.004	0.057	82	-
ξ	3.53	0.30	2.52	4.44	2809[a]	-
γ	0.51	0.17	0.06	1.05	108	
Y	0.23	0.18	−0.22	0.69	104	1.25 ± 0.46 (184)
S_{cdm} (nm^{-1})	0.0147	0.0014	0.0109	0.0198	106	0.015 ± 0.004 (814)
S_{cdm}'	6.76	0.60	5.10	8.99	106	6.97 ± 1.71 (814)
S_{nap} (nm^{-1})	0.0089	0.0008	0.0075	0.0118	59[a]	0.011 ± 0.003 (840)

[a]Calculated prior to surface weighted averaging.
[b]Calculated at 670 nm; 676 nm was not available.

Dissolved, particulate and nonalgal absorption are significantly higher in LIS, as are b_{bp} and Chl.

[22] As expected for a complex estuary, IOPs and biogeochemical properties exhibit high variability (Figures 3–5). Across the region, Chl, $a_{\min}(440)$, a_φ (676), $a_p(440)$, $b_p(440)$, $c_p(440)$ all vary by about two orders of magnitude, while $a_{nap}(440)$ varies by a factor of about 20 (Table 3).

[23] Spectral plots of three major IOPs, a_p, a_{cdm}, and b_{bp} (Figure 4), illustrate several broad trends in IOP magnitude and variability across subregions. Hudson River plume waters (NYB, dash-dotted line) have the highest a_p and a_{cdm} ($p < 0.01$), and the highest variability of all three parameters, followed by WLIS, the Connecticut River plume, CTR, CLIS and ELIS. Variability in a_{cdm} between, and within, subregions of LIS is generally very small (Figure 4), although this is not true of NYB plume waters which exhibit considerably higher a_{cdm} (and higher variability) than non-plume waters. Of the three bulk IOPs shown in Figure 4, b_{bp}

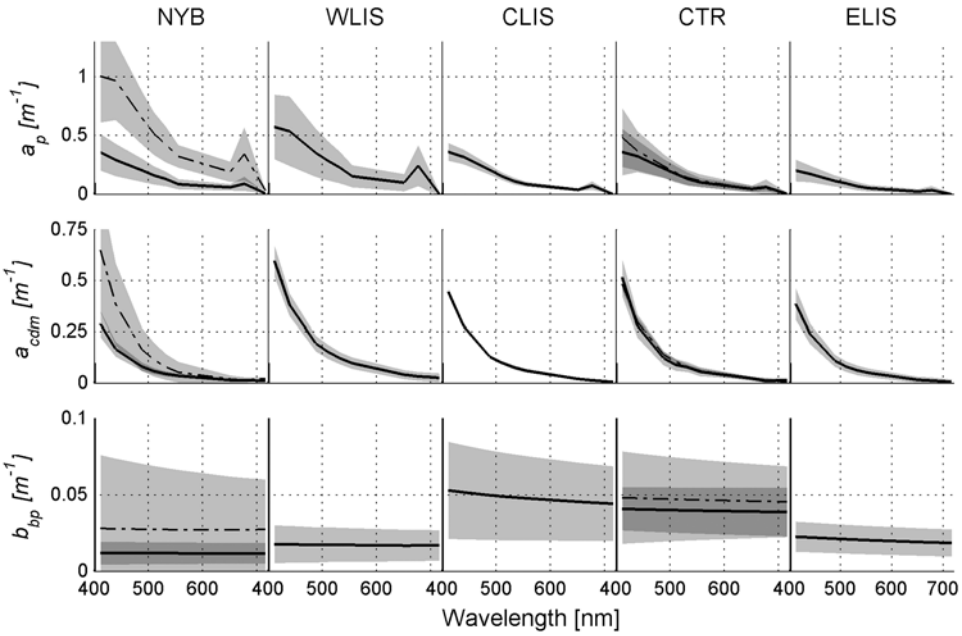

Figure 4. Subregionally averaged spectral particulate and dissolved absorption and particulate backscattering coefficients (solid line or dash-dotted line) showing variability (1 standard deviation; shaded region). For regions NYB and CTR, an additional dash-dotted line indicates data collected within the Hudson River (including the East River) or Connecticut River plumes, respectively.

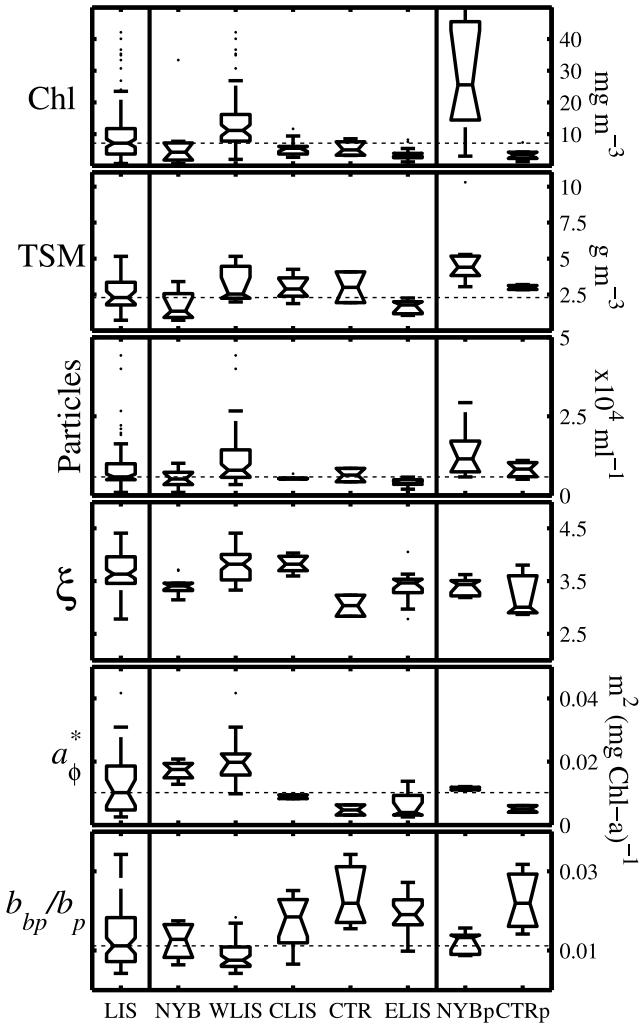

Figure 5. (middle) Chlorophyll, total suspended material, total particles (~6 – 230 μm), particle size distribution slope, phytoplankton specific absorption (676 nm), and backscattering ratio (650 nm) across the five subregions of the study area. (right) River plume data. (left) LIS averages across all subregions excluding river plume data.

has by far the highest variability within (and between) subregions. CTR plume waters (dash-dotted line in Figure 4) have the highest b_{bp}, followed by CLIS, and NYB plume. Plume waters in NYB also exhibit elevations in a_p, a_{cdm} and b_{bp}. CTR plume waters, on the other hand, while showing a small elevation and spectral flattening of b_{bp}, show very little change in a_p or a_{cdm}; the exception being enhanced particulate absorption in the blue deriving from NAP (Figure 4).

[24] ANOVA shows significant differences ($p < 0.01$) in optical properties and Chl between subregions where Chl, $b_{bp}(650)$, $a_{cdm}(440)$, $a_{nap}(440)$, a_φ (676) and $a_p(440)$ generally increase with proximity to either the head of the estuary, or, on a smaller geospatial scale, to the Connecticut River. Exceptions to this pattern can be found at four CLIS stations located in close proximity to New Haven harbor, and one station immediately outside Stratford harbor (Figure 1, northwest corner of central basin subregion). In these areas, the elevated backscattering ratio suggests higher suspended sediment loads that may result from urban run-off and deposition from the Quinnipiac and Housatonic rivers, which empty into New Haven and Stratford harbors. Another exception is at CTR, where IOPs are also principally driven by delivery of minerogenic materials rather than CDM or phytoplankton. Previous studies have shown that a_{cdm} correlated very well with salinity (r^2 as high as 0.94, $p < 0.001$) within individual watersheds in LIS [*Branco and Kremer*, 2005; *Branco*, 2007], but here we found that CDM absorption at 440 nm correlated only moderately with salinity over the entire region ($r^2 = 0.55$, $n = 109$, $p < 0.001$), and scatter about the conservative mixing line was approximately random (data not shown).

[25] Variability in Chl, a_φ and a_{nap} across the region can be very high *within* a given season, particularly in autumn and winter, but no significant differences were observed *between* seasons. Backscattering was found to be significantly lower ($p < 0.01$) in summer than spring or autumn, but not different from winter. Dissolved absorption is higher in summer than winter or spring, and most variable in autumn. Total particulate absorption is higher in summer than winter, but not different during any other times of year.

3.2. Ocean Color Parameters and Variability

[26] The ocean color parameters S_{cdm}, Y, and a_φ* are significantly lower in LIS than in the NOMAD data set (Figures 3 and 6). Differences in the ocean color parameters S_{cdm} and a_φ* are small between the two data sets, but Y is considerably lower in LIS (0.23 ± 0.18) than NOMAD (1.25 ±

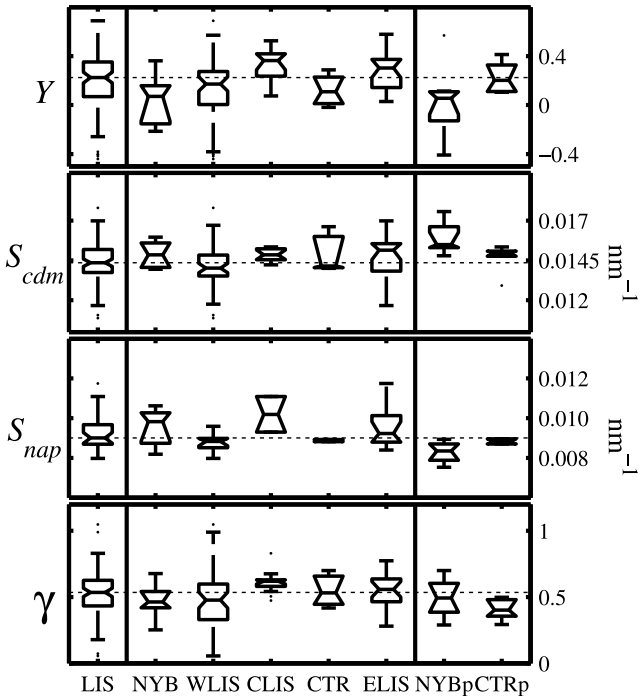

Figure 6. (middle) Backscattering slope, dissolved absorption slope, nonalgal particulate slope, and particle attenuation slope across the five subregions of the study area. (right) River plume data. (left) LIS averages across all subregions excluding river plume data.

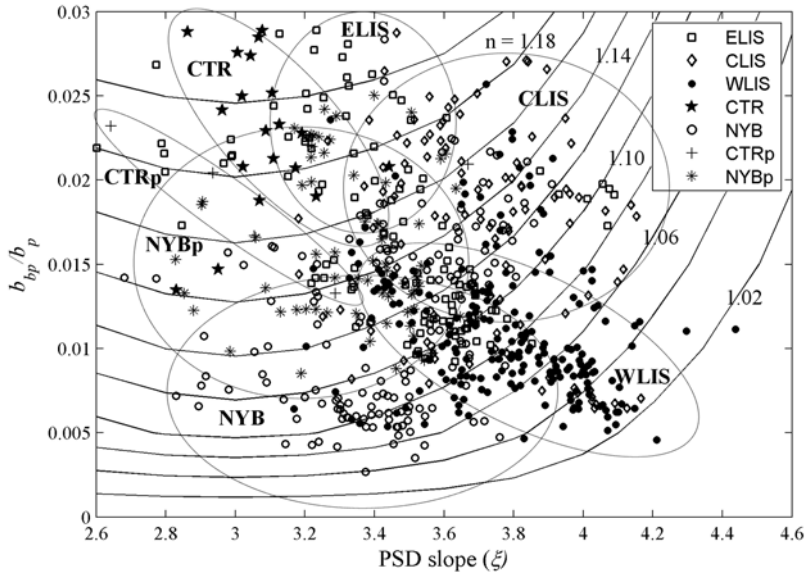

Figure 7. Backscattering ratio at 650 nm and particle size distribution slope by region (symbols) showing estimated bulk particulate refractive index (relative to seawater) modeled after *Twardowski and Donaghay* [2001].

0.46), which is not strictly limited to nearshore waters. This is perhaps not surprising given that backscattering by a population of large polydispersed particles, such as those found in estuarine waters, is believed to be approximately spectrally flat (i.e., $Y \approx 0$) [*Zaneveld and Kitchen*, 1995; *Babin et al.*, 2003a], while smaller particles and/or monodispersion, expected further from shore, leads to stronger spectral dependence and a correspondingly larger Y [e.g., *Morel and Ahn*, 1990]. Similar to many previous studies on the subject (see review by *Twardowski et al.* [2004]), we find that S_{cdm} has low spatial and temporal variability in LIS. Our median S_{cdm} (0.0147 ± 0.0014 nm^{-1}) is within the range (0.0145 nm^{-1} − 0.015 nm^{-1}) of what is considered a "typical" marine value from an historical perspective [*Twardowski et al.*, 2004] and within 2% of the global average reported in NOMAD, but fell below the values reported by *Babin et al.* [2003b] for the coastal waters around Europe (0.0176 ± 0.0020 nm^{-1}) and by *Tzortziou et al.* [2006] for the Chesapeake Bay (0.018 nm^{-1}).

[27] NOMAD does not contain measurements of the backscattering ratio $\tilde{b}_{bp}$, an indicator of the composition of suspended particles [*Ulloa et al.*, 1994]. LIS is characterized by fairly high $\tilde{b}_{bp}$ (555) (1.3% ± 0.8%), comparable to those found in the English Channel and North Sea (1.38% ± 0.83% [*Loisel et al.*, 2007]), the Gulf of California (~0.5% − ~2.0% [*Twardowski and Donaghay*, 2001]), Great Bay, New Jersey, and nearby shelf waters (0.5% − 3.5% [*Boss et al.*, 2004]). The backscattering ratio varies by a factor of about 15, and is only weakly correlated to Chl in LIS (r^2 = 0.23), a finding similar to the *Loisel et al.* [2007] study in the English Channel and North Sea, and does not follow earlier models [*Ulloa et al.*, 1994; *Morel and Maritorena*, 2001; *Twardowski and Donaghay*, 2001; *Sullivan et al.*, 2005], indicating that $\tilde{b}_{bp}$ is driven more by variability in suspended minerogenic material than by Chl. Furthermore, following the model of *Twardowski and Donaghay* [2001], we found that the combination of $\tilde{b}_{bp}$ and PSD slope, ξ, suggest a predominance of minerogenic particles with high bulk refractive index (relative to seawater, 1.12 ± 0.04) across the region (Figure 7).

[28] Within a 95% confidence interval, Y, S_{cdm}, S_{nap}, and γ have subregional population means which are not significantly different from the mean of the regional LIS population (Figure 6 (left)). Statistical differences are evident between only two individual subregions: Y is moderately higher in CLIS (0.36 ± 0.13) than NYB (−0.03 ± 0.24), and S_{cdm} is slightly lower in WLIS (0.0144 ± 0.0009 nm^{-1}) than in NYB plume waters (0.0153 ± 0.0009 nm^{-1}). However, values of Y can be qualitatively grouped into two categories depending on the degree of variability in Y and whether they fall above or below the complete data set median line (Figure 6, dotted horizontal line). The first group comprises LIS "open waters" consisting of ELIS, CLIS and WLIS which have a high backscattering slope with low variability ($Y = 0.32 \pm 0.128$), and the second comprises localized regions heavily influenced by rivers and nearshore resuspension, and consists of CTR, CTR plume, NYB, and NYB plume, which have a lower slope with very high variability (0.10 ± 0.20).

[29] PSD slope ξ is higher in CLIS and WLIS than elsewhere signifying a higher proportion of smaller particles. Seasonally, ξ is significantly lower in winter than spring or summer, signifying higher proportions of larger particles during winter months. Interestingly, no correlation was found between ξ and the particulate attenuation spectral slope, γ, as expected [*Voltz*, 1954; *Kitchen et al.*, 1982; *Barnard et al.*, 1998; *Boss et al.*, 2001]. This may be due to the lack of small particle (<6μm) data in the calculation of ξ from the PSD (see section 2.2.), while γ was calculated from c_p data for particles > 0.2 μm [*Boss et al.*, 2001]. *Kitchen et al.* [1982] found that in productive natural waters, particles < ~5 μm do not follow a hyperbolic shape, so omission of

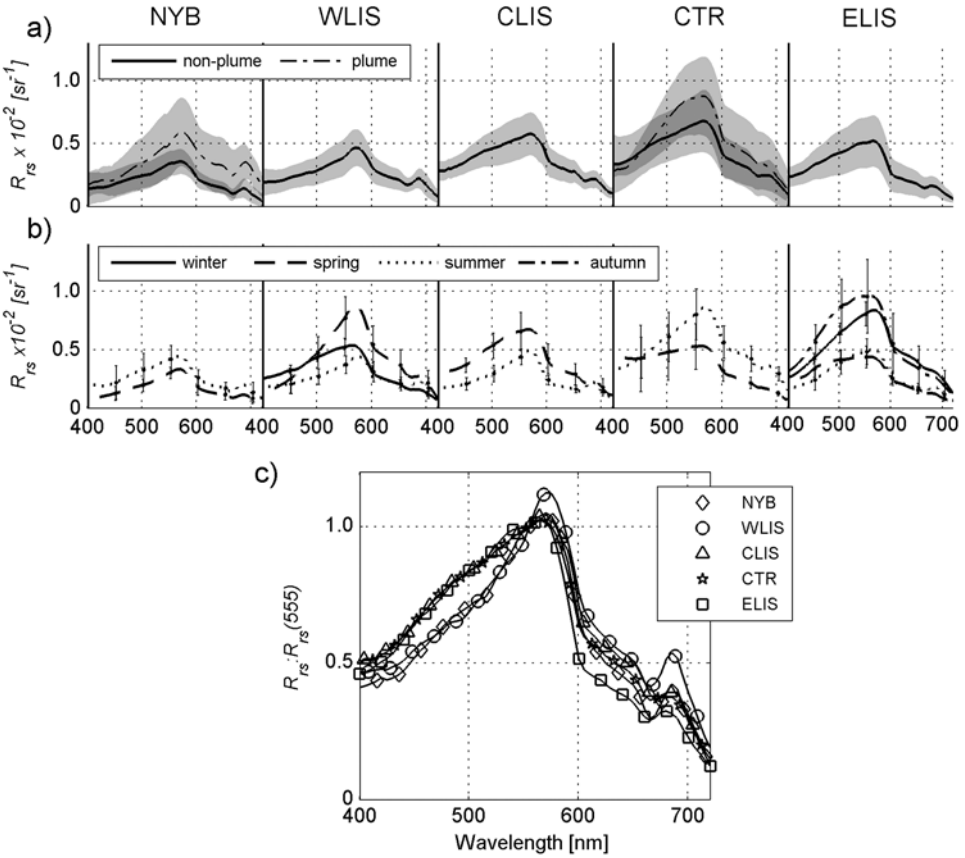

Figure 8. Observed remote sensing reflectance spectra. (a) Average (lines) spectra with variability (1 standard deviation; shaded region) shown for each subregion. (b) Subregional spectra averaged by season (lines) with variability (1 standard deviation; error bars). (c) Median spectra (normalized to 555 nm) showing differences in spectral shape between subregions.

these size classes seems justified when calculating ξ, though further study in this area is needed. Particulate backscattering slope, Y, correlated well with γ ($r^2 = 0.70$, rank 10).

[30] No differences between seasons are apparent in spectral shape parameters Y, S_{nap}, a_φ* or γ, but S_{cdm} appears lower in autumn than during the other seasons, which may be a result of seasonal riverine pulses delivering more labile CDM into LIS in autumn [e.g., *Carder et al.*, 1989].

3.3. Radiometric Properties and Variability

[31] Figure 8a shows average R_{rs} and variability (1 standard deviation) for each subregion, with plume stations shown separately. In general, all subregions exhibit typical estuarine reflectance signatures: low R_{rs} in the blue owing to high CDM, NAP and algal absorption, high R_{rs} in the green resulting from relatively high backscattering, and variable R_{rs} in the red depending on the level of phytoplankton absorption (~675 nm) and chlorophyll fluorescence (~685 nm). Reflectances are highest in the river plume regions where backscattering is elevated by suspended sediment (Figure 4), and lowest in WLIS and NYB where algal absorption is highest.

[32] Seasonal variability in R_{rs} is high in all subregions (Figure 8b). The highest overall reflectances were observed in autumn, although only one subregion (ELIS) was sampled during this season. The autumnal reflectances are characterized by a significant broadening in the green peak of R_{rs} resulting from enhanced suspended sediment backscattering coupled with relatively weak algal absorption in the blue. Other seasons do not appear to exhibit coherent trends in R_{rs}, except that summertime observations show a stronger algal signature: a more "peaked" green reflectance, with notable phytoplankton absorption near 675 nm and chlorophyll fluorescence near 685 nm.

[33] To assess variability in the shape of R_{rs} between subregions, $R_{rs}(\lambda)$ was scaled to $R_{rs}(555)$ (Figure 8c). Reflectance spectra can be separated into two classes based on spectral shape: algal and sediment driven. NYB and WLIS are algal driven with a highly peaked spectrum centered at 570 nm, similar to phytoplankton-induced red or brown "tides." The remaining subregions are characterized by broader peak reflectances characteristic of high minerogenic "clay-like" particles [*Dierssen et al.*, 2006, Figure 8c].

3.4. Optical Closure

[34] Overall, optical closure between measured and modeled $R_{rs}(\lambda)$ was good, with 53% of stations falling at ranks 1–2, 32% at ranks 3–4, and only 15% of stations ranking 5 or higher. Near-coastal and estuarine waters present particular challenges to optical closure. Studies by *Chang et al.* [2003] outside Great Bay, New Jersey, and *Tzortziou et al.* [2006] in the Chesapeake Bay both found

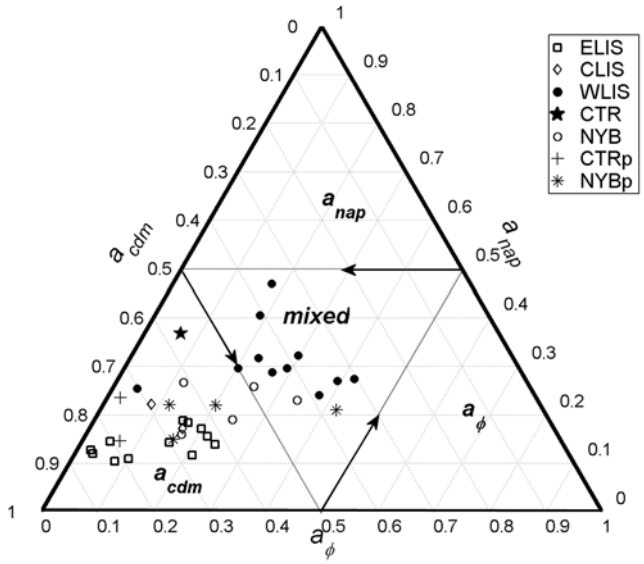

Figure 9. Ternary plot showing the budget of nonwater absorption components (dissolved, nonalgal, and phytoplankton) at 440 nm distinguished by subregion (symbols) for the 37 stations at which all of these components were measured. Internal triangles delimit three regions where each of the absorption components dominate and one mixed region. Arrows indicate axes from which grid lines originate.

that scattering corrections used in processing ac-9 data may have contributed to significant error in absorption measurements in these relatively turbid waters where near-infrared particulate absorption is often nonzero. They found that these errors lead to discrepancies in optical closure, because absorption measurements were propagated into model estimates of water leaving radiances by incorporation into the radiative transfer model. From spectrophotometric filterpad measurements in LIS, we found that on average $a_p(715) = 0.02 \pm 0.01$ m^{-1}, and $a_p(730) = 0.01 \pm 0.01$ m^{-1}, although accommodating these offsets (where possible) in the scattering corrections for the WetLabs instruments did not significantly improve our closure results. *Tzortziou et al.* [2006] furthermore showed that closure may be improved by accounting for spectral shape and depth profile differences in $\tilde{b}_{bp}$, and by using the a Fournier-Fourand (FF) phase function based on $\tilde{b}_{bp}$ to model the volume scattering function $\beta(\lambda, \theta)$ in Hydrolight. In LIS, we found that using an FF phase function based on field measurements of $\tilde{b}_{bp}$, rather than the Petzold 'average particle' volume scattering function [*Petzold*, 1972], was critical to good closure, but saw no improvement when depth variability in $\tilde{b}_{bp}$ was incorporated into the radiative transfer model.

4. Discussion

[35] Here we evaluate the diversity of the inherent optical properties and ocean color parameters in the region with respect to the delivery and distribution of optically significant constituents and identification of potential optical water types. Our observations show that LIS is an estuary in which Chl, TSM, light absorption, and scattering are not only exceptionally high compared with the NOMAD data set, but also highly variable from one location to another. The dynamic ranges and maximum values of the absorption coefficient, the backscattering ratio, and Chl, were found to be considerably higher in LIS (Table 3) than in nearby coastal and estuarine waters including coastal New Jersey [*Chang et al.*, 2002], the Gulf of Maine [*Balch et al.*, 2004], and the Chesapeake Bay [*Tzortziou et al.*, 2006]. Furthermore, sea surface reflectances, IOPs, and biogeochemical properties show that the region may comprise at least two optical domains: a phytoplankton-dominated regime (NYB and WLIS) and a sediment-dominated regime (remaining subregions). The former domain is characterized by spectral R_{rs} having strong algal characteristics, high Chl, high PSD slopes (Figure 7; i.e., more small particles), and low particulate backscattering ratios. The latter domain is characterized by larger particles with higher bulk refractive indexes (Figure 7; i.e., similar to those of clay [*Lide*, 1997]) as derived from $\tilde{b}_{bp}$ and ξ using the model of *Twardowski and Donaghay* [2001]. These two domains correspond well with the two cases (phytoplankton and inorganic) presented in the study by *Morel and Prieur* [1977], in which phytoplankton-dominated waters exhibited more peaked reflectance maxima in the green than those of sediment-dominated waters. In phytoplankton-dominated waters, strong chlorophyll and carotenoid absorption between ~400 − 500 nm and chlorophyll absorption centered at 675 nm leads to a "v-shaped" total absorption spectrum (resulting in a more peaked reflectance), while in sediment-dominated waters, enhanced backscattering across the spectrum combined with NAP absorption in the blue leads to a less peaked reflectance spectrum. Our results also show, however, that despite these two domains being present in LIS, the spectral quality of optically significant constituents (e.g., Y, S_{cdm}, S_{nap}, γ, a_φ*) is not significantly different regionally or seasonally.

4.1. Subregional Trends

[36] In eastern Long Island Sound (ELIS), where exchange with the continental shelf is vigorous, the water column has the lowest a_p and a_{cdm} in the region (Figure 4). Phytoplankton absorption and b_{bp} are also low compared with other subregions of LIS, though still significantly higher than those found in nearby continental shelf waters [*Gardner et al.*, 2001; *Sosik et al.*, 2001]. The dissolved constituent absorption in ELIS describes greater than 50% of all (nonwater) absorption in the blue portion of the spectrum (Figure 9). The combined effect of these attributes for ELIS is a green-peaked reflectance spectrum (Figure 8) that is somewhat broadened by enhanced backscattering (i.e., above shelf water conditions), particularly in late fall. This optical water mass is dominated by high concentrations of relatively large suspended sediments and low phytoplankton abundance as derived from PSD, $\tilde{b}_{bp}$, a_{nap}, a_φ, and Chl measurements (Figures 5, 7, and 8).

[37] Twenty kilometers west of the estuary mouth, the Connecticut River (CTR) flows into LIS carrying high sediment loads (e.g., high n_p and a_{nap}, low biomass, and a flattening in the R_{rs} peak) and concentrations of CDM comparable to regional averages (i.e., $a_{cdm}(440)$, Table 3). However, owing to large tidal excursions carrying LIS water far up into the Connecticut River with each semidiurnal tide, river plume conditions only episodically characterize the optical properties in the CTR subregion. *Ackleson* [2006]

suggested that relatively large particle aggregates within the CTR plume undergo disaggregation as a result of current shear at the lateral plume boundary. Our data appear to support this theory, showing a lower Y and ξ (i.e., larger particles) in the plume than in the adjacent waters. During plume events, sea surface reflectance is significantly enhanced in the green and red portion of the spectrum in response to increases in overall backscattering. Moreover, variability in R_{rs} observations is also influenced by seasonality that brings episodic run-off pulses of plume water. CDM represents about half of the absorption in the blue portion of the spectrum in this subregion (Figure 9), and is not notably enhanced during plume events in CTR (Figure 4). There was no significant change in S_{cdm} in CTR plume waters compared with adjacent CTR waters or regional averages, suggesting that CDM in the CT River has a similar chemical composition to LIS (e.g., fulvic to humic acid fraction) and has undergone a similar degree of degradation (e.g., photochemical bleaching) prior to entering LIS [*Bricaud et al.*, 1981; *Carder et al.*, 1989; *Mopper et al.*, 1991; *Roesler et al.*, 1989].

[38] The central basin (CLIS) experiences the competing influences of optical constituents from ELIS, WLIS and CTR. Large tidal excursions mix comparatively clear shelf waters with the turbid river discharge, and the productive WLIS waters. Furthermore, subtidal (residual) estuarine flow draws the outflow of the Connecticut River westward into CLIS along the north shore before driving it southward and eastward toward the Race [*Codiga and Aurin*, 2007], contributing to the variability in suspended sediment concentrations (as qualitatively estimated from bulk refractive index, a_{nap}, and TSM), b_{bp}, and $\tilde{b}_{bp}$ (e.g., Figures 4, 5, and 7). Figure 7 shows that particulates are comparatively small (high ξ), and span a fairly large range in refractive index ($\sim$1.06 − 1.20). However, in general, the optical and radiometric properties of CLIS are closest to region-wide averages, and have low overall variability.

[39] Western Long Island Sound (WLIS) has been studied intensively in recent decades in order to better characterize the factors influencing bottom water hypoxia [e.g., *Anderson and Taylor*, 2001; *O'Shea and Brosnan*, 2000; *Parker and O'Reilly*, 1991; *U.S. Environmental Protection Agency*, 1998]. Observations made during this study (e.g., Chl, a_{φ}, R_{rs}) agree with earlier findings that WLIS is the most phytoplankton rich area within LIS [*Anderson and Taylor*, 2001; *Connecticut Department of Environmental Protection (CTDEP)*, 2005]. High a_{φ} and a_{cdm} in the blue diminish blue reflectances leading to weaker, more sharply peaked R_{rs} spectra with distinctive a_{φ} absorption and Chl fluorescence signatures near 675 nm and 685 nm. While NAP absorption is elevated in WLIS above regional averages, the depressed backscattering ratio and particulate refractive index suggest that turbidity in WLIS is principally driven by phytoplankton biomass and associated detrital materials, rather than suspended sediments. Dissolved absorption is stronger in WLIS than elsewhere, principally due to delivery of CDM from the Hudson River (i.e., via the East River); a phenomenon common in many estuaries [*Jerlov*, 1953; *Siegel et al.*, 2002; *Stedmon and Markager*, 2003] and observed elsewhere in LIS [*Branco and Kremer*, 2005]. In fact, CDM levels in WLIS are similar to those found in Hudson River plume conditions (Figure 4). Measured S_{cdm} in NYB and WLIS plume waters (NYBp, 0.0155 ± 0.001 nm^{-1}) is higher than those of adjacent WLIS (i.e., nonplume, 0.0140 ± 0.0013 nm^{-1}, $p < 0.01$), and slightly higher than those considered "typical" of marine environments (0.0145 nm^{-1} − 0.0015 nm^{-1}) [*Twardowski et al.*, 2004]. *Carder et al.* [1989] showed that terrestrial and freshwater CDM is typically associated with a lower fulvic to humic acid fraction accompanied by a decrease in S_{cdm}. Hence, elevated NYBp S_{cdm} suggests a more refractory CDM pool which has undergone considerable photodegradation and a shift to smaller molecular weight CDM complexes absorbing at shorter wavelengths [*Del Vecchio and Blough*, 2002].

[40] Contrary to the open ocean, where increased Chl is often associated with a decrease in the chlorophyll-specific phytoplankton absorption [*Bricaud et al.*, 1995], we observe no significant trend in a_{φ}* with Chl across the region. Measured a_{φ}*(676) are low across LIS (0.01–0.02 m^2 (mg Chl a)$^{-1}$) consistent with a predominance of nano- and microplankton in the region [*Ciotti et al.*, 2002]. Studies by the CT Department of Environmental Protection demonstrated that the assemblage of diatoms, cryptophytes and dinoflagellates was similar across LIS and dominated by larger phytoplankton species (>20 μm) [*CTDEP*, 2005]. However, we find significantly higher a_{φ}* in the productive waters of WLIS (0.020 ± 0.010 m^2 (mg Chl a)$^{-1}$) compared to ELIS (0.010 ± 0.009 m^2 (mg Chl a)$^{-1}$) ($p < 0.01$, $n = 10$). WLIS is also characterized by a smaller average particle size (i.e., higher PSD slope ξ) compared with all other subregions except CLIS. Although not tested in this study, these results would be consistent with a higher background abundance of smaller ultra- and picoplankton in WLIS, which would serve to increase the bulk a_{φ}*, and may indicate an enhanced microbial loop in these productive waters [*Anderson and Taylor*, 2001; *CTDEP*, 2005].

[41] The New York Bight (NYB) subregion, here including New York Harbor and the East River, is the most optically diverse and variable subregion sampled, although variability is greatly reduced by isolation of stations sampled within river plume conditions (Figures 4–8). A study by *Johnson et al.* [2003] demonstrated that plume waters in the region were distinguished by larger contributions to absorption by NAP, and lower contributions by CDM. Our findings also show that plume conditions within NYB are characterized by high a_{nap}, but also exceptionally high a_p, a_{cdm}, and b_{bp}, resulting from enhanced Chl, TSM and total particle loads caused in part by urban run-off containing high particulate and nutrient concentrations [e.g., *Brosnan and O'Shea*, 1996]. The discrepancy between our findings and those of Johnson et al. with respect to absorption by CDM may be explained by the fact that they were contrasting Hudson River plume waters with upwelled waters along the New Jersey shore, whereas our study included stations throughout the region (as shown in Figure 1). An increase in S_{cdm} (as described above) was also observed in the plume waters of NYB accompanied by small decreases in S_{nap} and Y. Low values of a_{φ}* are consistent with the presence of large, bloom-forming diatoms common in this region. Modeled bulk particulate refractive indexes are slightly higher in plume (1.14 ± 0.03) than nonplume (1.09 ± 0.03) waters, suggesting that the region contains significant concentrations of both phytoplankton and suspended sediments.

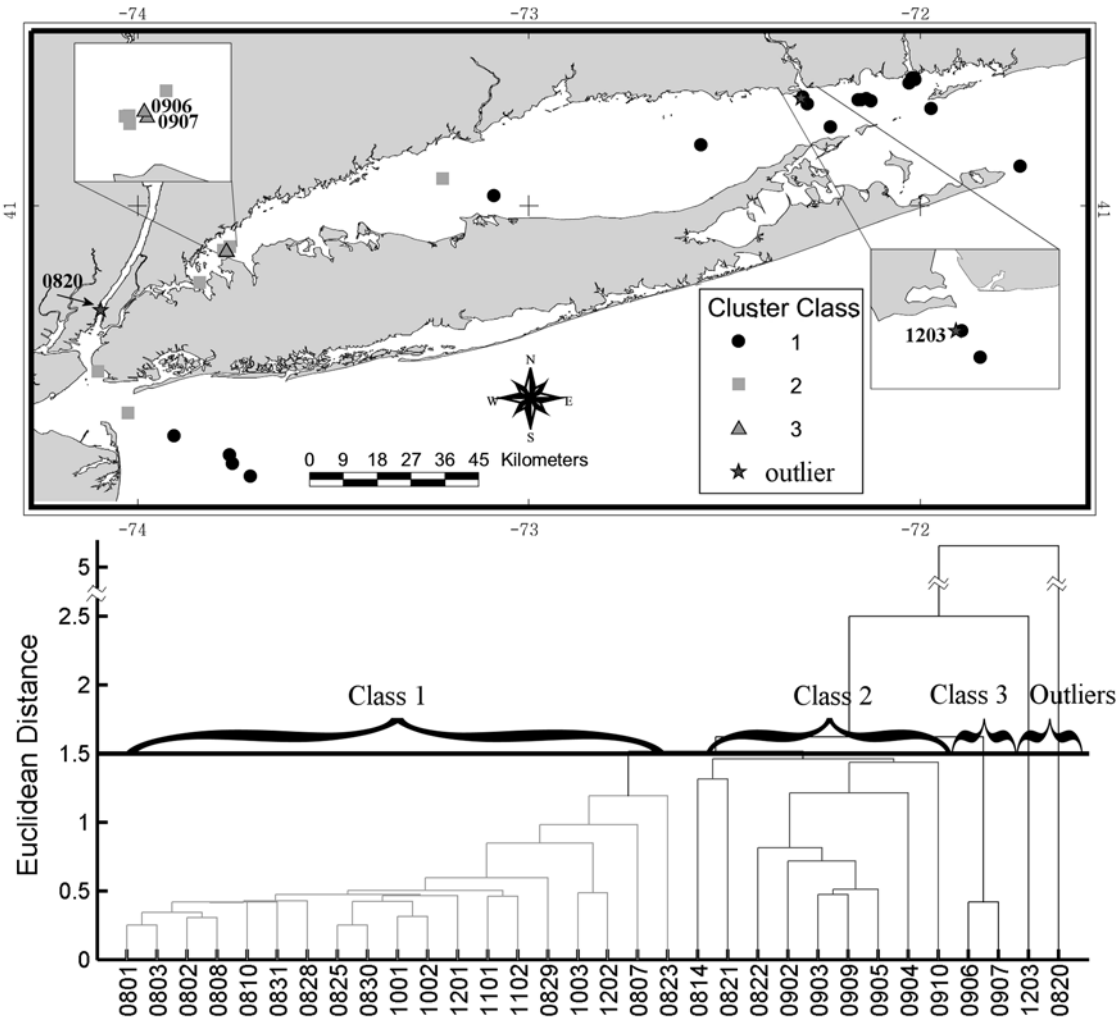

Figure 10. Clustering analysis for IOP magnitudes (i.e., $a_p(440)$, $a_\varphi(676)$, $a_{nap}(440)$, $a_{cdm}(440)$, $b_p(440)$). (top) Spatial distribution of clustered stations by class (symbol). Exceptional and class 3 stations have been identified by station number. (bottom) Dendrogram showing clustered stations with Euclidean distances and linkages between numbered stations (x axis). Taller linkages represent weaker linkages, or less similarity between stations.

4.2. Optical Water Types

[42] The classification of optical water types (defined operationally as waters with similar or covarying optical properties, ocean color parameters, and/or biogeochemical properties) can be valuable or even necessary for optimizing ocean color algorithm performance. The simplest example of this is the convention that operational empirical satellite algorithms for retrieving Chl may be classified as valid only in Case 1 waters in which optical properties are dominated by phytoplankton [*Morel and Prieur*, 1977], i.e., generally waters outside of the influence of terrigenous inputs. Identification of optical water types within a region may also facilitate an explanation for some of the variability in optical properties, particularly in highly dynamic coastal and estuarine environments.

[43] We have shown that a considerable degree of the observed variability in IOPs and biogeochemical properties in LIS is attributable to subregional effects such as riverine suspended sediment delivery and high productivity in areas of high nutrient loading. One technique for assessing whether these influences lead to discrete optical regimes within LIS is to evaluate the absorption budgets of the normalized absorption components (i.e., $a_{cdm} + a_\varphi + a_{nap} = 1$) [*Morel and Prieur*, 1977; *Prieur and Sathyendranath*, 1981]. For example, an absorption budget at 440 nm (where all three components absorb strongly) derived by *Oubelkheir et al.* [2006] for the Fitzroy Estuary and Keppel Bay waters in northeastern Australia showed a pattern in which phytoplankton absorption was increasingly dominant moving offshore, while the inverse was true of NAP absorption. In contrast, a ternary plot of the absorption budgets for each of the 37 stations in LIS at which all of these components were measured reveals two basic regimes (Figure 9). Productive WLIS, NYB and most Hudson River plume waters have higher contributions of a_φ and a_{nap}, and reside closer to the central "mixed" portion of the plot. ELIS, CLIS and the CT River are centered near the bottom left corner of the plot and dominated by CDM. Compared with absorption budgets

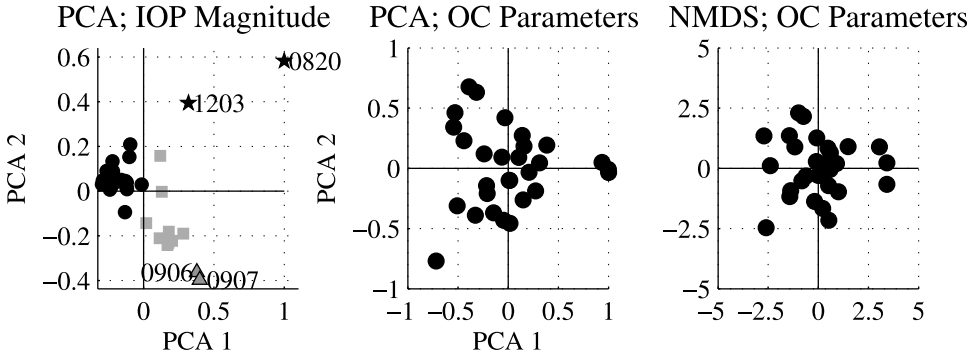

Figure 11. Multivariate statistical analysis with hierarchical clustering based on (left) IOP magnitudes (i.e., $a_p(440)$, $a_\varphi(676)$, $a_{nap}(440)$, $a_{cdm}(440)$, $b_p(440)$, and $b_{bt}(650)$) and (middle and right) ocean color parameters (i.e., S_{cdm}, S_{nap}, Y, γ, and a_φ*(676)). Principal component analysis distribution and clusters (symbols same as in Figure 10) are shown in Figures 11 (left) and 11 (middle) and nonmetric multidimensional scaling in Figure 11 (right).

(at 443 nm) for various coastal water bodies around Europe, this pattern most closely resembles that of the North Sea [*Babin et al.*, 2003b].

[44] *Van Der Woerd and Pasterkamp* [2004, 2008] described how remote sensing retrievals of IOPs and Chl could be improved for the North Sea and Dutch coast through a characterization of optical water type based on combinations of IOPs normalized to their respective constituent concentrations (specific IOPS), such as the chlorophyll-specific phytoplankton absorption coefficient used in this study. A critical component of this methodology is to establish distinct and discrete optical water types within a data set. Following a similar approach to that used by *Brando et al.* [2006] and *Blondeau-Patissier et al.* [2009] to establish optical domains in the coastal waters of northeastern Australia, multivariate ordination statistics are performed both on collective measures of IOPs, and on ocean color parameters.

[45] The cluster analysis based on IOP magnitudes (i.e., $a_p(440)$, a_φ (676), $a_{nap}(440)$, $a_{cdm}(440)$, $b_p(440)$, and $b_{bt}(555)$) show three geographic groups (Figure 10 (top)): 1) the first (and largest) cluster consists of stations distributed throughout LIS and offshore portions of NYB (i.e., stations generally furthest from direct fluvial influence), 2) consists of stations in WLIS and New York Harbor, and 3) consists of stations in WLIS exhibiting exceptionally high phytoplankton absorption at 676 nm (0.352 – 0.378 m^{-1}). The dendrogram (Figure 10 (bottom)) shows individual linkages and the Euclidean distance at which cluster discrimination occurs (1.5) for stations at which all properties were measured (n = 32, closure rank 5). The high cophenet correlation coefficient (0.93) indicates that distances in ordination space are a faithful representation of the original data distances. Selection of the Euclidean distance threshold is somewhat arbitrary, and clearly the linkage between the two largest clusters is relatively strong (indicated by short vertical lines in the dendrogram), meaning that while they are distinct, they are not nearly as different from each other as they are from the third cluster, or from the exceptional stations which do not cluster into any of the three groups. Two exceptional stations (stations which did not fit into any cluster) are also identified: 0820 (Hudson River plume), and 1230 (Connecticut River plume). These stations highlight two optical end-members in LIS representing the two major sources of terrigenous input into LIS (the Hudson and Connecticut rivers). A plot of the first two principal components (explaining > 90% of the observed variance in IOP magnitudes) shows a continuum of the three clusters, and the isolated end-member stations (Figure 11 (left)). PCA coefficients are all positive in the first principal component indicating it is a weighted average of the IOP magnitudes. NMDS stress is low (0.03), and clustering shows a nearly identical pattern to PCA (data not shown).

[46] A very different story emerges from the results of ordination statistics based on ocean color parameters (i.e., S_{cdm}, S_{nap}, Y, γ, a_φ*(676)). Briefly, clustering fails to identify distinct clusters of stations with similar attributes, and all stations cluster together (Figure 11 (middle), cophenet correlation 0.76). The first two principal components explain < 70% of the variance in ocean color parameters, therefore data are also displayed in NMDS space to more accurately illustrate ordinate data distances within the single cluster (Figure 11 (right)). This result reinforces our earlier finding based on ANOVA comparisons, namely that ocean color parameters have low variability across the region.

5. Summary

[47] By distinguishing properties determined by the magnitude (or concentration) of optical constituents (IOPs) found in LIS waters from those which describe its spectral qualities (ocean color parameters), and then subjecting each to multivariate ordination and hierarchical clustering analysis, we found that the underlying spectral characteristics are relatively stable across all subregions of LIS throughout the year. Variability in the magnitudes of optical properties can largely be explained by proximity to sources of turbidity (such as riverine deposits of NAP and CDM) and areas with high productivity (i.e., in the eutrophic subregion of WLIS and New York Harbor), and to a lesser degree on seasonal changes. The absorption coefficient at most stations is dominated by CDM, although stations in the eutrophic area of WLIS and NYB also have significant contributions of a_φ and a_{nap}. Stations tended to cluster into four groups on the basis of IOPs (i.e., a_p, a_φ, a_{nap}, a_{cdm}, b_p, and b_{bt}), representing highly productive areas (centered in WLIS), turbid productive areas (centered around New York City), optically

intermediate areas distributed throughout the open waters of LIS and extending offshore into NYB, and the distinct end-members representing the Connecticut and Hudson rivers plumes.

[48] Clustering analysis and ordination statistics fail to discern any stations or clusters of stations which could be characterized as having a distinct optical water type based on ocean color parameters (i.e., S_{cdm}, S_{nap}, Y, γ, a_{φ}*(676)). With very few exceptions, subregional statistical comparison (ANOVA) of these parameters also support this conclusion. Exceptions can be found (e.g., in S_{cdm} and Y) in highly localized areas associated within the Connecticut and Hudson River plumes. Stability in ocean color parameters will facilitate parameterization of semianalytical ocean color algorithms for the region, as dynamic subregional parameterization will not be required.

[49] Discrete measurements of inherent and apparent optical properties provide a foundation for understanding the physical and biogeochemical processes of this complex estuary, as shown in this study. However, ocean color satellite imagery, when properly processed, has the potential for greatly enhancing our observational perspective by providing kilometer or better resolution of surface water properties synoptically. The results of such an effort would allow for enhanced monitoring and characterization of this important estuary over time. Future research will focus on applying the results of this study to developing new approaches for ocean color remote sensing in the region.

[50] **Acknowledgments.** This work was funded in part by the Department of Defense National Defense Science and Engineering Graduate Fellowship, National Aeronautic and Space Administration's Ocean Biology and Biogeochemistry research program (NNG04GN61G to H.M. Dierssen), and the University of Connecticut. Many thanks to the Long Island Sound Integrated Coastal Observation System (LISICOS) and the crew on the R/V *Connecticut*, to Scott Freeman for providing optical field data, and to Emmanuel Boss and Steve Ackleson for equipment and ship time provided in support of the project.

References

Ackleson, S. (2006), Optical determinations of suspended sediment dynamics in western Long Island Sound and the Connecticut River plume, *J. Geophys. Res.*, *111*, C07009, doi:10.1029/2005JC003214.

Anderson, T. H., and G. T. Taylor (2001), Nutrient pulses, plankton blooms, and seasonal hypoxia in western Long Island Sound, *Estuaries*, *24*(2), 228–243, doi:10.2307/1352947.

Astoreca, R., K. Ruddick, V. Rousseau, B. Van Mol, J.-Y. Parent, and C. Lancelot (2006), Variability of the inherent and apparent optical properties in a highly turbid coastal area: Impact on the calibration of remote sensing algorithms, *EARSeL eProceedings*, *5*, 1–17.

Babin, M., A. Morel, V. Fournier-Sicre, F. Fell, and D. Stramski (2003a), Light scattering properties of marine particles in coastal and open ocean waters as related to the particle mass concentration, *Limnol. Oceanogr.*, *48*(2), 843–859.

Babin, M., D. Stramski, G. M. Ferrari, H. Claustre, A. Bricaud, G. Obolensky, and N. Hoepffner (2003b), Variations in the light absorption coefficients of phytoplankton, nonalgal particles, and dissolved organic matter in coastal waters around Europe, *J. Geophys. Res.*, *108*(C7), 3211, doi:10.1029/2001JC000882.

Balch, W., D. T. Drapeau, B. C. Bowler, E. S. Booth, J. I. Goes, A. Ashe, and J. M. Frye (2004), A multi-year record of hydrographic and bio-optical properties in the Gulf of Maine: Part I. Spatial and temporal variability, *Prog. Oceanogr.*, *63*, 57–98, doi:10.1016/j.pocean.2004.09.003.

Barnard, A. H., W. S. Pegau, and J. R. V. Zaneveld (1998), Global relationships of the inherent optical properties of the oceans, *J. Geophys. Res.*, *103*(C11), 24,955–24,968, doi:10.1029/98JC01851.

Blondeau-Patissier, D., V. E. Brando, K. Oubelkheir, A. G. Dekker, and P. Daniel (2009), Bio-optical variability of the absorption and scattering properties of the Queensland inshore and reef waters, Australia, *J. Geophys. Res.*, *114*, C05003, doi:10.1029/2008JC005039.

Blumberg, A. F., and D. W. Pritchard (1997), Estimates of the transport through the East River, New York, *J. Geophys. Res.*, *102*(C3), 5685–5703, doi:10.1029/96JC03416.

Boss, E., and W. S. Pegau (2001), Relationship of light scattering at an angle in the backward direction to the backscattering coefficient, *Appl. Opt.*, *40*(30), 5503–5507, doi:10.1364/AO.40.005503.

Boss, E., W. S. Pegau, W. D. Gardner, J. R. V. Zaneveld, A. H. Barnard, M. S. Twardowski, G. C. Chang, and T. D. Dickey (2001), Spectral particulate attenuation and particle size distribution in the bottom boundary layer of a continental shelf, *J. Geophys. Res.*, *106*(C5), 9509–9516, doi:10.1029/2000JC900077.

Boss, E., W. S. Pegau, M. Lee, M. Twardowski, E. Shybanov, G. Korotaev, and F. Baratange (2004), Particulate backscattering ratio at LEO 15 and its use to study particle composition and distribution, *J. Geophys. Res.*, *109*, C01014, doi:10.1029/2002JC001514.

Bowers, D. G., G. E. L. Harker, and B. Stephan (1996), Absorption spectra of inorganic particles in the Irish Sea and their relevance to remote sensing of chlorophyll, *Int. J. Remote Sens.*, *17*, 2449–2460, doi:10.1080/01431169608948782.

Branco, A. B. (2007), Empirical methods for the prediction of optical properties in shallow estuaries, Ph.D. thesis, Univ. of Conn., Groton, Conn.

Branco, A. B., and J. N. Kremer (2005), The relative importance of chlorophyll and colored dissolved organic matter (CDOM) to the prediction of the diffuse attenuation coefficients in shallow estuaries, *Estuaries*, *28*(5), 643–652, doi:10.1007/BF02732903.

Brando, V. E., D. Blondeau-Patissier, A. G. Dekker, P. Daniel, J. Anstee, M. Wettle, K. Oubelkheir, and C. Lesley (2006), Bio-optical variability of Queensland coastal waters for parameterization of coastal-reef algorithms, paper presented at Ocean Optics XVIII Conference, Soc. of Photo-Opt. Instrum. Eng., Montreal, Canada.

Bricaud, A., A. Morel, and L. Prieur (1981), Absorption by dissolved organic matter of the sea (yellow substance) in the UV and visible domains, *Limnol. Oceanogr.*, *26*(1), 43–53, doi:10.4319/lo.1981.26.1.0043.

Bricaud, A., M. Babin, A. Morel, and H. Claustre (1995), Variability in the chlorophyll-specific absorption coefficients of natural phytoplankton: Analysis and parameterization, *J. Geophys. Res.*, *100*(C7), 13,321–13,332, doi:10.1029/95JC00463.

Brosnan, T. M., and M. L. O'Shea (1996), Long-term improvements in water quality due to sewage abatement in the lower Hudson River, *Estuaries*, *19*(4), 890–900, doi:10.2307/1352305.

Burg, R. (Ed.) (2008), Sound health: A report on the status and trends of the Long Island Sound, report, N. Engl. Interstate Water Pollut. Control Comm., Stamford, Conn.

Carder, K. L., R. G. Steward, G. R. Harvey, and P. B. Ortner (1989), Marine humic and fulvic acids: Their effects on remote sensing of chlorophyll, *Limnol. Oceanogr.*, *34*, 68–81, doi:10.4319/lo.1989.34.1.0068.

Carder, K. L., F. R. Chen, Z. P. Lee, S. K. Hawes, and D. Kamykowski (1999), Semianalytic Moderate-Resolution Imaging Spectrometer algorithms for chlorophyll a and absorption with bio-optical domains based on nitrate-depletion temperatures, *J. Geophys. Res.*, *104*(C3), 5403–5421, doi:10.1029/1998JC900082.

Chang, G. C., T. D. Dickey, O. Schofield, A. D. Weidemann, E. Boss, W. S. Pegau, M. A. Moline, and S. Glenn (2002), Nearshore physical processes and bio-optical properties in the New York Bight, *J. Geophys. Res.*, *107*(C9), 3133, doi:10.1029/2001JC001018.

Chang, G. C., T. D. Dickey, C. D. Mobley, E. Boss, and W. S. Pegau (2003), Toward closure of upwelling radiance in coastal waters, *Appl. Opt.*, *42*(9), 1574–1582, doi:10.1364/AO.42.001574.

Chang, G. C., A. H. Barnard, and J. R. V. Zanefeld (2007), Optical closure in a complex coastal environment: Particle effects, *Appl. Opt.*, *46*(31), 7679–7692, doi:10.1364/AO.46.007679.

Ciotti, A. M., M. R. Lewis, and J. J. Cullen (2002), Assessment of the relationships between dominant cell size in natural phytoplankton communities and the spectral shape of the absorption coefficient, *Limnol. Oceanogr.*, *47*(2), 404–417.

Codiga, D. L., and D. A. Aurin (2007), Residual circulation in eastern Long Island Sound: Observed transverse-vertical structure and exchange transport, *Cont. Shelf Res.*, *27*, 103–116, doi:10.1016/j.csr.2006.09.001.

Coleman, J. E. (1999), *Optical Variability of the Chesapeake Bay*, edited by T. S. P. Report, U.S. Nav. Acad., Annapolis.

Connecticut Department of Environmental Protection (CTDEP) (2005), Monitoring phytoplankton community composition in Long Island Sound with HPLC photopigment profiles, fact sheet, Hartford.

Del Vecchio, R., and N. V. Blough (2002), Photobleaching of chromophoric dissolved matter in natural waters: Kinetics and modeling, *Mar. Chem.*, *78*, 231–253, doi:10.1016/S0304-4203(02)00036-1.

Dierssen, H. M., R. M. Kudela, J. P. Ryan, and R. C. Zimmerman (2006), Red and black tides: Quantitative analysis of water-leaving radiance and perceived color for phytoplankton, color dissolved organic matter, and suspended sediments, *Limnol. Oceanogr.*, *51*(6), 2646–2659.

Etheridge, S. M., and C. Roesler (2004), Temporal variation in phytoplankton, particulates, and colored dissolved material based on optical properties during a Long Island brown tide compared to an adjacent embayment, *Harmful Algae*, *3*, 331–342, doi:10.1016/j.hal.2004.06.005.

Fargion, G. S., and J. L. Mueller (2000), Ocean optics protocols for satellite ocean color sensor validation, revision 2, *Rep. NASA/TM-2000-209966*, Goddard Space Flight Cent., Greenbelt, Md.

Fournier, G. R., and J. L. Forand (1994), Analytic phase function for ocean water, in *Ocean Optics XII*, edited by J. S. Jaffe, pp. 194–201, Soc. of Photo-Opt. Instrum. Eng., Bellingham, Wash.

Gardner, W. D., et al. (2001), Optics, particles, stratification, and storms on the New England continental shelf, *J. Geophys. Res.*, *106*(C5), 9473–9497, doi:10.1029/2000JC900161.

Garver, S. A., and D. A. Siegel (1997), Inherent optical property inversion of ocean color spectra and its biogeochemical interpretation: 1. Time series from the Sargasso Sea, *J. Geophys. Res.*, *102*(C8), 18,607–18,625, doi:10.1029/96JC03243.

Gay, P. S., J. O'Donnell, and C. A. Edwards (2004), Exchange between Long Island Sound and adjacent waters, *J. Geophys. Res.*, *109*, C06017, doi:10.1029/2004JC002319.

Gordon, H. R., and K. Ding (1992), Self-shading of in-water optical instruments, *Limnol. Oceanogr.*, *37*(3), 491–500.

Gordon, H. R., and A. Morel (1983), *Remote Sensing of Ocean Color for Interpretation of Satellite Visible Imagery*: A Review, Springer, New York.

Gotelli, N. J., and A. M. Ellison (2004), *A Primer of Ecological Statistics*, Sinauer Assoc., Sunderland, Mass.

Gould, R. W., R. A. Arnone, and M. Sydor (2001), Absorption, scattering; and remote-sensing reflectance relationships in coastal waters: Testing a new inversion algorithm, *J. Coastal Res.*, *17*(2), 328–341.

Gregg, M. C., and K. L. Carder (1990), A simple spectral solar irradiance model for cloudless maritime atmospheres, *Limnol. Oceanogr.*, *35*(8), 1657–1675, doi:10.4319/lo.1990.35.8.1657.

Hogg, R. V., and J. Ledolter (1987), *Engineering Statistics*, MacMillan, New York.

Holm-Hansen, O., C. J. Lorensen, R. W. Holmes, and J. D. Strickland (1965), Fluorometric determination of chlorophyll, *J. Cons. Cons. Int. Explor. Mer*, *30*, 3–15.

Jerlov, N. G. (1953), Influence of suspended and dissolved matter on the transparency of sea water, *Tellus*, *5*, 59–65.

Johnson, D. R., J. Miller, and O. Schofield (2003), Dynamics and optics of the Hudson River outflow plume, *J. Geophys. Res.*, *108*(C10), 3323, doi:10.1029/2002JC001485.

Kirk, J. T. O. (1994), *Light and Photosynthesis in Aquatic Ecosystems*, doi:10.1017/CBO9780511623370, Cambridge Univ. Press, New York.

Kitchen, J. C., J. R. V. Zaneveld, and H. Pak (1982), Effect of particle size distribution and chlorophyll content on beam attenuation spectra, *Appl. Opt.*, *21*(21), 3913–3918, doi:10.1364/AO.21.003913.

Kramer, C. Y. (1956), Extension of multiple range tests to group means with unequal number of replications, *Biometrics*, *12*(3), 307–310, doi:10.2307/3001469.

Kruskal, J. B., and M. Wish (1978), *Multidimensional Scaling: Quantitative Applications in the Social Science*, Sage, Newbury Park, Calif.

Leathers, R. A., C. S. Roesler, and N. J. McCormick (1999), Ocean inherent optical property determination from in-water light field measurements, *Appl. Opt.*, *38*(24), 5096–5103, doi:10.1364/AO.38.005096.

Lee, Z. P., K. L. Carder, and R. A. Arnone (2002), Deriving inherent optical properties from water color: A multiband quasi-analytical algorithm for optically deep waters, *Appl. Opt.*, *41*(27), 5755–5772, doi:10.1364/AO.41.005755.

Lide, D. R. E. (Ed.) (1997), Physical and optical properties of minerals, in *CRC Handbook of Chemistry and Physics*, 77th ed., pp. 4130–4136, CRC Press, Boca Raton, Fla.

Loisel, H., X. Meriaux, J.-F. Berthon, and A. Poteau (2007), Investigation of the optical backscattering to scattering ratio of marine particles in relation to their biogeochemical composition in the eastern English Channel and southern North Sea, *Limnol. Oceanogr.*, *52*(2), 739–752.

Maritorena, S., D. A. Siegel, and A. R. Peterson (2002), Optimization of a semianalytical ocean color model for global-scale applications, *Appl. Opt.*, *41*(15), 2705–2714, doi:10.1364/AO.41.002705.

Mobley, C. D. (1994), *Light and Water: Radiative Transfer in Natural Waters*, Academic, San Diego, Calif.

Moore, C. M., M. I. Lucas, R. Sanders, and R. Davidson (2005), Basin-scale variability of phytoplankton bio-optical characteristics in relation to bloom state and community structure in the northeast Atlantic, *Deep Sea Res. Part I*, *52*(3), 401–419, doi:10.1016/j.dsr.2004.09.003.

Mopper, K., Z. Xianliang, R. J. Kieber, D. J. Kieber, R. J. Sikorski, and R. D. Jones (1991), Photochemical degradation of dissolved organic carbon and its impact on the ocean carbon cycle, *Nature*, *353*, 60–62, doi:10.1038/353060a0.

Morel, A., and Y. Ahn (1990), Optical efficiency factors of free-living marine bacteria: Influence of bacterioplankton upon the optical properties and particulate organic carbon in oceanic waters, *J. Mar. Res.*, *48*, 145–175, doi:10.1357/002224090784984632.

Morel, A., and A. Bricaud (1981), Theoretical results concerning light absorption in a discrete medium and application to the specific absorption of phytoplankton, *Deep Sea Res.*, *28*, 1375–1393, doi:10.1016/0198-0149(81)90039-X.

Morel, A., and S. Maritorena (2001), Bio-optical properties of oceanic waters: A reappraisal, *J. Geophys. Res.*, *106*(C4), 7163–7180, doi:10.1029/2000JC000319.

Morel, A., and L. Prieur (1977), Analysis of variations in ocean color, *Limnol. Oceanogr.*, *22*(4), 709–722, doi:10.4319/lo.1977.22.4.0709.

Morrison, J. R., and H. M. Sosik (2002), Inherent optical properties in New England coastal waters: Decomposition into contributions from optically important constituents, in *Ocean Optics XVI*, edited by S. Ackleson and C. Trees, pp. 1–10, Off. of Nav. Res., Santa Fe, N. M.

Morrison, R. E. (1970), Experimental studies on the optical properties of sea water, *J. Geophys. Res.*, *75*(3), 612–628, doi:10.1029/JC075i003p00612.

Mueller, J. L., and R. W. Austin (1995), Ocean optics protocols for SeaWiFS validation, *Tech. Memo. 104566*, NASA, Greenbelt, Md.

O'Donnell, J., H. G. Dam, W. F. Bohlen, and I. Babb (2007), LISICOS: The Long Island Sound integrated coastal observing system, interim report, Univ. of Conn., Groton, Conn.

O'Shea, M. L., and T. M. Brosnan (2000), Trends in indicators of eutrophication in western Long Island Sound and the Hudson-Raritan Estuary, *Estuaries*, *23*(6), 877–901, doi:10.2307/1353004.

Oubelkheir, K., L. A. Clementson, I. T. Webster, P. W. Ford, A. G. Dekker, L. C. Radke, and P. Daniel (2006), Using inherent optical properties to investigate biogeochemical dynamics in a tropical macrotidal coastal system, *J. Geophys. Res.*, *111*, C07021, doi:10.1029/2005JC003113.

Parker, C. A., and J. E. O'Reilly (1991), Oxygen depletion in Long Island Sound: A historical perspective, *Estuaries*, *14*(3), 248–264, doi:10.2307/1351660.

Petzold, T. J. (1972), Volume scattering functions for selected ocean waters, final technical report, pp. 72–78, Scripps Inst. of Oceanogr., San Diego, Calif.

Pope, R. M., and E. S. Fry (1997), Absorption spectrum (380–700 nm) of pure water. Part 2. Integrating cavity measurements, *Appl. Opt.*, *36*(33), 8710–8723, doi:10.1364/AO.36.008710.

Prieur, L., and S. Sathyendranath (1981), An optical classification of coastal and oceanic waters based on the specific absorption curves of phytoplankton pigments, dissolved organic matter, and other particulate materials, *Limnol. Oceanogr.*, *26*(4), 671–689, doi:10.4319/lo.1981.26.4.0671.

Riley, G. A. (1956), Oceanography of Long Island Sound 1952–1954, *Bull. Bingham Oceanogr. Collect.*, *15*, 8–49.

Roesler, C. S. (1998), Theoretical and experimental approaches to improve the accuracy of particulate absorption coefficients derived from the quantitative filter technique, *Limnol. Oceanogr.*, *43*(7), 1649–1660.

Roesler, C. S., and M. J. Perry (1995), In-situ phytoplankton absorption, fluorescence emission, and particulate backscattering spectra determined from reflectance, *J. Geophys. Res.*, *100*(C7), 13,279–13,294, doi:10.1029/95JC00455.

Roesler, C. S., M. J. Perry, and K. L. Carder (1989), Modelling in situ phytoplankton absorption from total absorption spectra in productive inland marine waters, *Limnol. Oceanogr.*, *34*(8), 1510–1523.

Siegel, D. A., S. Maritorena, and N. B. Nelson (2002), Global distribution and dynamics of colored dissolved and detrital organic materials, *J. Geophys. Res.*, *107*(C12), 3228, doi:10.1029/2001JC000965.

Sosik, H. M., R. E. Green, W. S. Pegau, and C. Roesler (2001), Temporal and vertical variability in optical properties of New England shelf waters during late summer and spring, *J. Geophys. Res.*, *106*(C5), 9455–9472, doi:10.1029/2000JC900147.

Stedmon, C. A., and S. Markager (2003), Behavior of the optical properties of coloured dissolved organic matter under conservative mixing, *Estuarine Coastal Shelf Sci.*, *57*, 973–979, doi:10.1016/S0272-7714(03)00003-9.

Sullivan, J. M., M. S. Twardowski, P. L. Donaghay, and S. A. Freeman (2005), Use of optical scattering to discriminate particle types in coastal waters, *Appl. Opt.*, *44*(9), 1667–1680, doi:10.1364/AO.44.001667.

Sullivan, J. M., M. Twardowski, J. R. V. Zanefeld, C. M. Moore, A. H. Barnard, P. L. Donaghay, and B. Rhoades (2006), Hyperspectral temperature and salt dependencies of absorption by water and heavy water in the 400–750 nm spectral range, *Appl. Opt.*, *45*(21), 5294–5309, doi:10.1364/AO.45.005294.

Twardowski, M. S., and P. L. Donaghay (2001), Separating in situ and terrigenous sources of absorption by dissolved materials in coastal waters, *J. Geophys. Res.*, *106*(C2), 2545–2560, doi:10.1029/1999JC000039.

Twardowski, M. S., J. M. Sullivan, P. L. Donaghay, and J. R. V. Zaneveld (1999), Microscale quantification of the absorption by dissolved and particulate material in coastal waters with an ac-9, *J. Atmos. Oceanic Technol.*, *16*(6), 691–707, doi:10.1175/1520-0426(1999)016<0691:MQOTAB>2.0.CO;2.

Twardowski, M. S., E. Boss, J. M. Sullivan, and P. L. Donaghay (2004), Modeling the spectral shape of absorption by chromophoric dissolved organic matter, *Mar. Chem.*, *89*(1–4), 69–88, doi:10.1016/j.marchem.2004.02.008.

Tzortziou, M., J. R. Herman, C. L. Gallegos, P. J. Neale, A. Subramaniam, L. W. Harding, and Z. Ahmad (2006), Bio-optics of the Chesapeake Bay from measurements and radiative transfer closure, *Estuarine Coastal Shelf Sci.*, *68*, 348–362, doi:10.1016/j.ecss.2006.02.016.

Ulloa, O., S. Sathyendranath, and T. Platt (1994), Effect of particle size-distribution on the backscattering ratio in seawater, *Appl. Opt.*, *33*, 7070–7077, doi:10.1364/AO.33.007070.

U.S. Environmental Protection Agency (1998), Long Island Sound study: Phase III actions for hypoxia management, *Rep. EPA 902-R-98-002*, Stamford, Conn.

Van Der Woerd, H., and R. Pasterkamp (2004), Mapping of the North Sea turbid coastal waters using SeaWiFS data, *Can. J. Rem. Sens.*, *30*(1), 44–53.

Van Der Woerd, H., and R. Pasterkamp (2008), HYDROPT: A fast and flexible method to retrieve chlorophyll-a from multispectral satellite observations of optically complex coastal waters, *Remote Sens. Environ.*, *112*, 1795–1807, doi:10.1016/j.rse.2007.09.001.

Voltz, F. (1954), Die optik und meterologie der atmospharischen trubung, *Ber. Dtsch. Wetterdienstes*, *2*, 2–47.

Werdell, P. J., and S. W. Bailey (2005), An improved in situ bio-optical data set for ocean color algorithm development and satellite data product validation, *Remote Sens. Environ.*, *98*(1), 122–140, doi:10.1016/j.rse.2005.07.001.

Werdell, P. J., and C. S. Roesler (2003), Remote assessment of benthic substrate composition in shallow waters using multispectral reflectance, *Limnol. Oceanogr.*, *48*, 557–567.

Whitmire, A. L., E. Boss, T. J. Cowles, and W. S. Pegau (2007), Spectral variability of the particulate backscattering ratio, *Opt. Express*, *15*(11), 7019–7031, doi:10.1364/OE.15.007019.

Zaneveld, J. R. V., and J. C. Kitchen (1995), The variation in the inherent optical-properties of phytoplankton near an absorption peak as determined by various models of cell structure, *J. Geophys. Res.*, *100*(C7), 13,309–13,320, doi:10.1029/95JC00451.

Zaneveld, J. R. V., J. C. Kitchen, and C. M. Moore (1994), Scattering error correction of reflecting-tube absorption meters, in *Ocean Optics XII*, edited by J. S. Jaffe, pp. 44–55, Soc. of Photo-Opt. Instrum. Eng., Bellingham, Wash.

Zaneveld, J. R. V., A. H. Barnard, and E. Boss (2005), Theoretical derivation of the depth average of remotely sensed optical parameters, *Opt. Express*, *13*(22), 9052–9061, doi:10.1364/OPEX.13.009052.

Zaneveld, J. R. V., A. H. Barnard, and Z. P. Lee (2006), Why are inherent optical properties needed in ocean-colour remote sensing?, in *Remote Sensing of Inherent Optical Properties: Fundamentals, Tests of Algorithms and Applications*, edited by Z. P. Lee, pp. 3–10, Int. Ocean Colour Coord. Group, Dartmouth, Nova Scotia.

D. A. Aurin and H. M. Dierssen, Department of Marine Sciences, University of Connecticut, Groton, CT 06340, USA. (dirk.aurin@uconn.edu)

M. S. Twardowski, WET Labs Inc., 165 Dean Knauss Dr., Narragansett, RI 02882, USA.

C. S. Roesler, Department of Geology, Bowdoin College, Brunswick, ME 04011, USA.